IEEE Open Journal of Control Systems

Received 8 January 2026; revised 16 March 2026; accepted 5 April 2026. Date of publication 24 April 2026; date of current version 8 May 2026. Recommended by Senior Editor Peter Seiler.

Digital Object Identifier 10.1109/OJCSYS.2026.3685925

Health-Aware Economic Model Predictive Control of Wave Energy Converters Based on a Reliability Metric

AMIN ZIAEI (Student Member, IEEE), HAFIZ AHSAN SAID, AND JOHN V. RINGWOOD (Life Fellow, IEEE)

Centre for Ocean Energy Research (COER), Department of Electronic Engineering, Maynooth University, W23 F2H6, Kildare, Ireland

CORRESPONDING AUTHOR: AMIN ZIAEI (e-mail: amin.ziaei.2024@mumail.ie).

This work was supported in part by Taighde Éireann (Research Ireland) under Grant 21/FFP-A/8997 and in part the Marine Renewable Ireland (MaREI) Centre under Grant 12/RC/2302_P2.

ABSTRACT Conventionalenergy-maximising controllers for wave energy converters (WECs) often exaggerate device motion, which can shorten device lifetime and increase operational costs (OpEx), by reducing maintenance intervals and system reliability. This paper proposes a novel health-aware WEC controller to achieve a suitable trade-off between captured energy and device lifetime, ultimately leading to a lower levelised cost of energy (LCoE). Using a reliability metric, the proposed controller incorporates power take-off degradation into the performance function of an economic model predictive controller (EMPC). The proposed performance function does not require additional (regularisation) terms to convexify the optimisation problem, as is often necessary for typical energy-maximising WEC EMPCs. Simulation results demonstrate the effectiveness of the proposed controller in achieving an optimal trade-off between captured energy and device longevity. Furthermore, this study examines potential challenges in the implementation of health-aware control for WECs and outlines key directions for future research in the health-aware WEC control domain.

INDEX TERMS Economic model predictive control, health-aware control, reliability, wave energy converters.

NOMENCLATURE

Abbreviations

EMPC	Economic model predictive control.
MOO	Multi-objective optimisation.
MTTF	Mean time to failure.
PTO	Power take-off.
RUL	Remaining useful life.
WEC	Wave energy converter.

Symbols

m	Mass of the buoy [kg].
$\eta(t)$	Free-surface elevation [m].
$\mathbf{x_r}(t)$	State vector of the radiation subsystem.
$\mathbf{x}(t)$	State vector of the WEC model.
$f_{pto}(t)$	Power take-off force [N].
$E_c(t)$	Captured mechanical energy [J].
$f_{ex}(t)$	Wave excitation force [N].
$f_{pto}^{ref}(t)$	Reference power take-off force generated by a hydrodynamic controller (control input) [N].
$f_{re}(t)$	Restoring force [N].
$f_r(t)$	Radiation force [N].
m_∞	Added mass at infinite frequency [kg].
n_r	Dimension of radiation state-space model.
$R(t)$	Reliability index.
s_h	Hydrostatic restoring coefficient [N/m].
t	Time [s].
$z(t), \dot{z}(t), \ddot{z}(t)$	Heave displacement [m], velocity [m/s] and acceleration [m/s^2].

I. INTRODUCTION

The diminishing availability of fossil fuel reserves has led to a widespread understanding that these traditional energy sources will soon be unreliable. Therefore, researchers and

policymakers have focused on more reliable, sustainable, alternatives, such as renewable energy resources. Renewable energy resources are not only replenishable but also have a significantly lower carbon footprint compared to fossil fuels. Additionally, their extraction and utilisation result in fewer negative environmental impacts, making them a more sustainable choice for meeting our energy needs [1]. Despite numerous positive attributes of using renewable resources, energy-harnessing technologies for each resource are not at the same technology readiness level (TRL) [2]. Focusing on wave energy technology, although ocean waves have the potential to generate approximately 32,000 TW/year of energy [3] and provides complementarity benefits [4], [5], the wave energy industry is still in the early stages, resulting in a higher levelised cost of energy (LCoE), compared to other renewable energy industries, such as wind [6]. Aiming to reach a lower LCoE for wave energy technology has driven the design of hundreds of wave energy converters [7]. However, despite the diverse range of designs, achieving economic competitiveness remains a challenge. This is where advanced control strategies become critical, as they significantly improve the efficiency and economic viability of wave energy devices, by maximizing energy extraction [8].

Generally, wave energy converters (WECs) are devices converting the mechanical energy of ocean waves to electricity through a power take-off (PTO) system. From a control system perspective, to design a controller for a WEC, LCoE is the primary control objective function to consider,[1] generally defined over a project/device/array lifetime based on capital costs (CapEx), operational costs (OpEx) and captured mechanical energy (E_c) [9] as:

$$\begin{cases} \text{LCoE} = \frac{\text{CapEx}+\text{PV(OpEx)}}{\text{PV}(E_c)}, \\ \text{PV(Q)} = \sum_{y_r=y_r^0}^{Y_r} \frac{\text{Q}(y_r)}{(1+R_d/100)^{y_r}}, \end{cases} \tag{1}$$

where the discount rate is denoted as R_d, with the project duration in years represented by Y_r. The term PV refers to the present value of a given quantity, such as Q.

In addition, E_c is defined as:

$$E_c = \int_0^{\mathsf{T}} \dot{z}(t) f_{pto}(t) dt, \quad t \in [0, T] \tag{2}$$

where $f_{pto}(t)$ is the control force, generated by a PTO, and $\dot{z}(t)$ is device velocity (see Section II for more detail).

Nevertheless, LCoE is not an entirely suitable control objective for designing a WEC controller. The reason is that OpEx is generally challenging to compute, due to a high level of uncertainty [6]. In addition, controllers need to take action in seconds, while OpEx is typically calculated in years [10]. Therefore, published studies usually take the denominator of the LCoE in (1), E_C, as a *surrogate measure* of LCoE, while assuming that OpEx is independent of E_c. In this way, the LCoE minimisation problem is transformed into an E_c maximisation problem. A WEC controller is designed to satisfy the energy-maximisation problem by exaggerating device motion, which can lead to device degradation (shorter lifetime) and subsequent increase in OpEx [11]. Note that the present work focuses on control-dependent PTO degradation during operational (power-producing) sea states. As illustrated by the phase-space example in Fig. 1, a WEC control law can drive the device to larger motion/velocity excursions (within the allowable operational envelope), thereby increasing PTO loading and accelerating degradation accumulation (see [11] for more detail). Nevertheless, WEC operation in extreme sea states can precipitate failures and can therefore be handled by a higher-level *supervisory control* layer that performs mode switching (e.g., power production versus survival) based on sea-state severity.

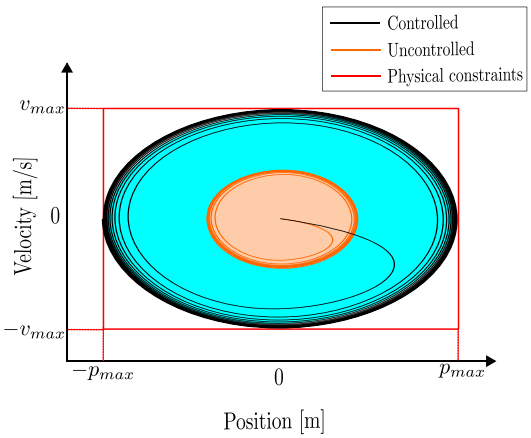

FIGURE 1. Operational (phase) space of an uncontrolled and controlled WEC device where p_{max} and v_{max} are the maximum position and velocity values, respectively. Inspired by [11].

The wave energy literature is replete with a wide variety of WEC controllers, from simple frequency-domain controllers [12] to advanced control structures, such as economic model predictive control (EMPC) [13], [14], [15], pseudo-spectral controllers [16], [17], and moment-based controllers [18], [19], [20]. However, to the best knowledge of the authors, few health-aware control methods have been proposed for WECs. Generally, health-aware control incorporates system-health information into the control design, which can be done using deterministic health metrics obtained from direct online health monitoring (e.g., accumulated fatigue damage), or using probabilistic health metrics (e.g., reliability) derived from operational data and a failure-rate model [21]. Recently, in [22], a general health-aware control structure is proposed for WECs, as depicted in Fig. 2. In the first step, a control-aware version of LCoE in (1) is achieved by considering a constant CapEx $= c$, then OpEx is linked by an unknown function F to a real-time lifetime metric $\chi(f_{pto})$, such as accumulated fatigue damage, remaining useful life (RUL), or reliability, described in detail in [23].

[1]Note that, for most renewable energy sources, including wave energy, the cost of the raw 'fuel' is zero, but the cost of conversion is not.

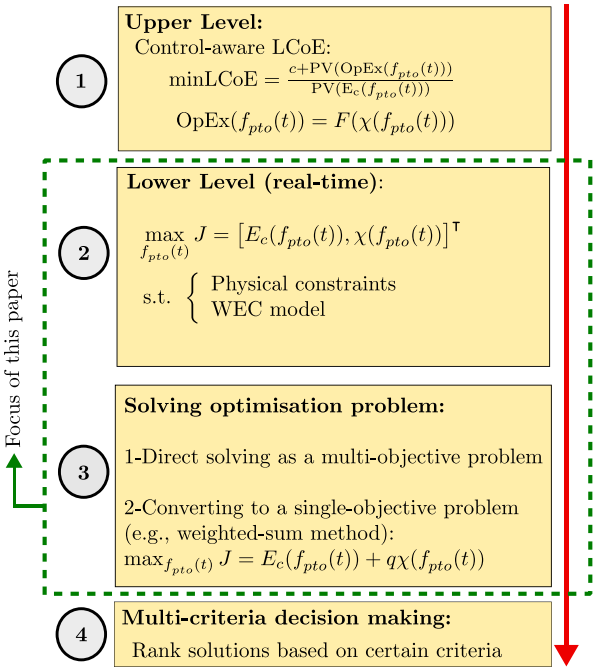

FIGURE 2. Structure of health-aware control problem. Inspired by [22].

Next, the real-time multi-objective optimisation problem can be solved directly or indirectly, by obtaining a single-objective optimisation problem using a decomposition method such as weighted-sum [24]. Finally, optimal solutions are ranked by a multi-decision-making algorithm. The current paper explores the development of a novel health-aware controller within the general framework illustrated in Fig. 2. It is worth noting that a new health-aware control paradigm, termed health-aware control augmentation, has recently been introduced in [25], [26], where an existing nominal (energy-maximising) control law is modified using WEC health information. However, as reported in [25], the simple augmentation structure does not provide reliable constraint satisfaction in irregular waves. Motivated by this limitation, the present paper develops the first optimisation-based health-aware WEC controller, based on EMPC, in the health-aware control structure, depicted Fig. 2, which explicitly enforces constraints and thereby guarantees constraint-handling performance. In addition, unlike the majority of energy-maximising EMPCs, which require an additional term for convexification of the optimal control problem [27], [28], the proposed health-aware EMPC inherently achieves convexification through the lifetime metric $\chi(f_{pto})$, which is integrated into the health performance function depicted in Fig. 2.

The remainder of the paper is organised as follows: Section II recalls fundamental concepts of WEC hydrodynamic modelling, and a WEC state-space model with a degrading PTO is obtained. A novel health-aware EMPC is developed in Section III, based on the health-aware control structure presented in Fig. 2. Simulation results for the proposed controller are presented in Section IV, and, finally, concluding remarks are provided in Section V.

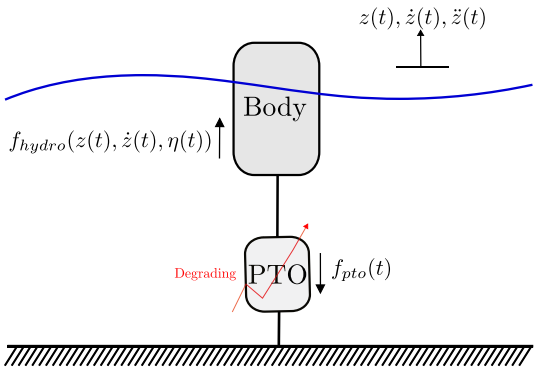

FIGURE 3. Simplified illustration of a wave energy converter with a degrading PTO, operating in a single (heave) degree of freedom.

II. DYNAMIC MODELLING OF A WEC

In this section, the fundamental concepts of WEC modelling are first briefly reviewed, and then state-space models, considering an ideal (healthy) or a degrading PTO, are obtained.

Consider a single-body wave energy converter, depicted in Fig. 3, which is fixed to the sea bed and only can oscillate in heave. If assumptions related to linear potential flow theory are considered, such as incompressible, inviscid and irrotational flow [29], [30], a linear hydrodynamic formulation for the WEC in Fig. 3, using Newton's second law, can be written as:

$$m\ddot{z}(t) = f_{hydro}(z(t), \dot{z}(t), \eta(t)) - f_{pto}(t), \tag{3}$$

where $z(t)$, $\dot{z}(t)$, and $\ddot{z}(t)$ are the displacement, velocity, and acceleration of the device, respectively. m is the mass of the buoy, $\eta(t)$ is the free-surface elevation, $f_{pto}(t)$ is the control force provided by a PTO, and $f_{hydro}(z(t), \dot{z}(t), \eta(t))$ is the superposition of all hydrodynamic forces, interacting with the device depicted in Fig. 3. $f_{hydro}(z(t), \dot{z}(t), \eta(t))$ can be written [31] based on radiation ($f_r(t)$), restoring ($f_{re}(t)$), and wave excitation ($f_{ex}(t)$) forces as:

$$f_{hydro}(z(t), \dot{z}(t), \eta(t)) = f_r(\ddot{z}(t), \dot{z}(t)) + f_{re}(z(t)) + f_{ex}(\eta(t)), \tag{4}$$

where

$$\begin{cases} f_r(\ddot{z}(t), \dot{z}(t)) = -m_\infty \ddot{z}(t) - k_r(t) * \dot{z}(t), \\ f_{re}(z(t)) = -s_h z(t), \\ f_{ex}(\eta(t)) = \eta(t) * k_e(t). \end{cases} \tag{5}$$

In (5), $k_r(t)$ and $k_e(t)$ are the radiation and excitation impulse functions, respectively. m_∞ is the added mass at infinite frequency, s_h is the hydrostatic restoring coefficient, and $*$ represents the convolution operator.

Remark 1: It is worth noting that $f_r(\ddot{z}(t), \dot{z}(t))$ and $f_{re}(z(t))$ in (5) are solely dependent on system states (i.e., position and velocity), while $f_{ex}(\eta(t))$ is purely a function of η, meaning that $f_{ex}(\eta(t))$ can be treated as an external disturbance in the state-space model. Nevertheless, the convolution term in the $f_r(\ddot{z}(t), \dot{z}(t))$ definition is a barrier to achieving a WEC state-space model. Therefore, as typically common

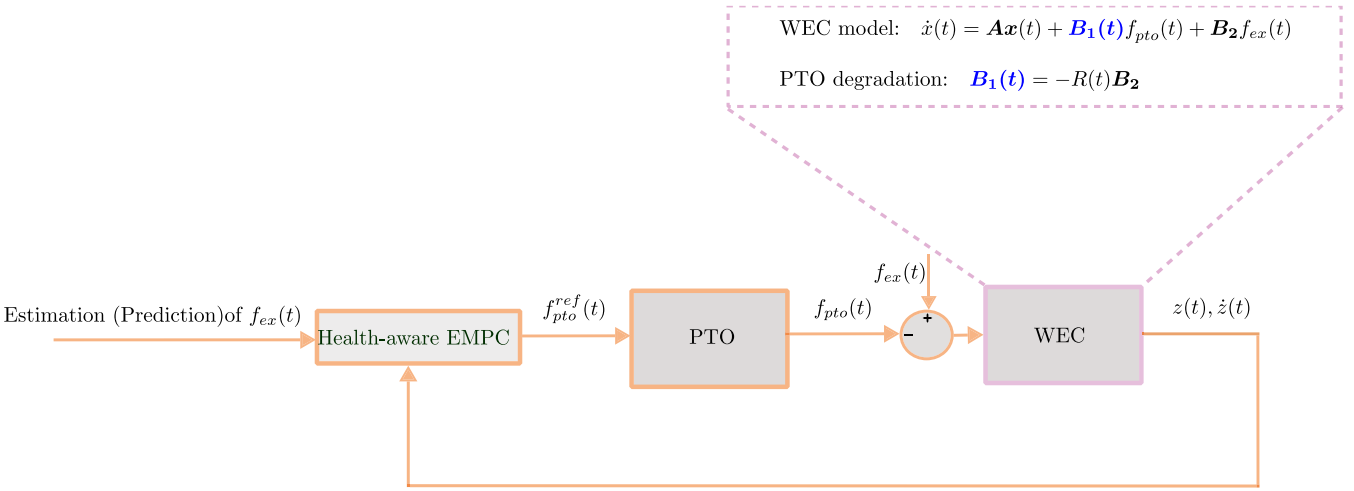

FIGURE 4. The closed-loop control system, considering PTO degradation.

in the literature, the convolution term (i.e., $k_r(t) * \dot{z}(t)$) is parametrised as a linear, strictly proper subsystem [9] as follows:

$$\begin{cases} \dot{\boldsymbol{x_r}}(t) = \boldsymbol{A_r}\boldsymbol{x_r}(t) + \boldsymbol{B_r}\dot{z}(t), \\ k_r(t) * \dot{z}(t) \approx \boldsymbol{C_r}\boldsymbol{x_r}(t), \end{cases} \tag{6}$$

where $\boldsymbol{x_r}(t) \in \mathbb{R}^{n_r \times 1}$, with n_r representing the radiation subsystem dimension, is the radiation subsystem state vector, and $\boldsymbol{A_r}$, $\boldsymbol{B_r}$ and $\boldsymbol{C_r}$ are state, input and output matrices with suitable dimensions.

A. WEC STATE-SPACE REPRESENTATION WITH AN IDEAL POWER TAKE-OFF

Consider Fig. 4, showing the closed-loop system block diagram. Based on the PTO block, the PTO input is a reference signal, such as $f_{pto}^{ref}(t)$, which a hydrodynamic controller generates. The output of the PTO is $f_{pto}(t)$, which represents the actual force applied to the WEC. The relationship between $f_{pto}^{ref}(t)$ and $f_{pto}(t)$, can be defined as follows:

Definition 1: The PTO electrical dynamics and the associated inner-loop current controller are assumed to operate on a time scale much faster than the hydrodynamic control loop. Therefore, at the hydrodynamic sampling rate, the commanded PTO force is tracked accurately, i.e.,

$$f_{pto}(t) = f_{pto}^{ref}(t),$$

and henceforth $f_{pto}(t)$ is taken as the control input (i.e., a separate reference $f_{pto}^{ref}(t)$ is not used).[2]

In addition, PTO degradation is defined as follows:

Definition 2: [PTO degradation] When the PTO is subject to degradation, the control matrix, $\boldsymbol{B}_1(t)$, becomes time-varying to reflect the evolving PTO condition. In contrast, for a healthy PTO, the control matrix is constant, i.e., $\boldsymbol{B}_1(t) = \boldsymbol{B}_1$.

[2]See, e.g., [32] for more detail regarding current controller.

Therefore, considering (3), (4), (5), **Remark** 1, **Definition** 1, and **Definition** 2, one can obtain the following linear time-invariant (LTI) state-space model when the PTO is healthy:

$$\begin{cases} \dot{\boldsymbol{x}}(t) = \boldsymbol{A}\boldsymbol{x}(t) + \boldsymbol{B_1} f_{pto}(t) + \boldsymbol{B_2} f_{ex}(t), \\ y_v(t) = \boldsymbol{C_v}\boldsymbol{x}(t), \quad y_z(t) = \boldsymbol{C_z} x(t), \end{cases} \tag{7}$$

where $\boldsymbol{x}(t) = [z(t), \dot{z}(t), \boldsymbol{x_r}(t)]^\intercal = [x_1(t), x_2(t), \boldsymbol{x_r}(t)]^\intercal \in \mathbb{R}^{(n_r+2)\times 1}$, and

$$\begin{cases} \boldsymbol{A} = \begin{bmatrix} 0 & 1 & \boldsymbol{0}_{1\times n_r} \\ -\frac{s_h}{(m+m_\infty)} & 0 & -\frac{\boldsymbol{C_r}}{(m+m_\infty)} \\ \boldsymbol{0}_{n_r\times 1} & \boldsymbol{B_r} & \boldsymbol{A_r} \end{bmatrix} \in \mathbb{R}^{(n_r+2)\times(n_r+2)}, \\ \boldsymbol{B_1} = -\boldsymbol{B_2} = \begin{bmatrix} 0 \\ -\frac{1}{(m+m_\infty)} \\ \boldsymbol{0}_{n_r\times 1} \end{bmatrix} \in \mathbb{R}^{(n_r+2)\times 1}, \\ C_z = \begin{bmatrix} 10\boldsymbol{0}_{1\times n_r} \end{bmatrix}, \\ C_v = \begin{bmatrix} 01\boldsymbol{0}_{1\times n_r} \end{bmatrix} \in \mathbb{R}^{1\times(n_r+2)}. \end{cases}$$

B. WEC STATE-SPACE REPRESENTATION WITH A DEGRADING POWER TAKE-OFF

Based on **Definition** 2, when the PTO is degrading, $\boldsymbol{B}_1(t) \neq -\boldsymbol{B}_2$. Therefore, it is necessary to obtain a mathematical mapping between $\boldsymbol{B}_1(t)$ and $\boldsymbol{B_2}$ to get a WEC state-space model representing PTO degradation. In Section II-B1, a lifetime metric, such as reliability, defines this mathematical mapping. Then, in Section II-B2, a state-space model for a degrading PTO, based on reliability is achieved.

1) RELIABILITY MODELLING

In this section, reliability is considered as a lifetime metric, since reliability, with the help of a reliability block diagram, can evaluate overall system degradation rather than

specific subsystem degradation, compared to accumulated fatigue damage [23] (e.g., accumulated fatigue damage of the hydraulic cylinder shaft of the point absorber in [33]). In addition, remaining useful life (RUL) can be calculated, based on reliability, if failure thresholds of components are available [34], [35].

Reliability, in general, is defined as the ability of a component to perform its needed function over a certain period, under given environmental and operational conditions [36]. Mathematically, reliability is represented as the probability of a component *not* failing over a specific period:

$$R(t) = e^{-\int_0^t \lambda(t)dt}, \quad R \in [0, 1] \tag{8}$$

where $\lambda(t)$ represents the failure rate [1/(unit of time)]. Different mathematical representations can be considered for $\lambda(t)$, based on component characteristics. Nevertheless, in control systems, if the considered component is an actuator (i.e., a PTO in this instance), $\lambda(t)$ can be defined as a function of the control input (i.e., $f_{pto}(t)$) [37], [38] as:

$$\lambda(t) = \lambda_0 L(f_{pto}(t)), \tag{9}$$

where $L(.)$ is the so-called *load function*, and λ_0 is the baseline (nominal) failure rate. It is worth noting that reliability assessment can be performed with or without knowledge of nominal failure-rate data. For components that comprise mechanical/electrical subcomponents for which nominal failure-rate information is typically available or can be estimated (e.g., PTO), the failure-rate model $\lambda(t)$ can be parametrised directly from λ_0 as shown in (9). In contrast, for structural components, nominal failure rates are typically unavailable; in such cases, reliability is commonly assessed using limit-state modelling with probabilistic uncertainty propagation (e.g., using Monte Carlo simulations), as discussed in [39]. Reliability-aware control methods based on known nominal failure-rate assessment have been investigated in various applications in the literature, including unmannedaerial vehicles (UAVs) [40], [41], wind turbines [42], and drinking water systems [43], [44].

In this paper, similar to [41], [43], the load function ($L(f_{pto}(t))$) is constructed based on the absolute value of the control input ($f_{pto}(t)$) as:

$$\lambda(t) = \lambda_0 \left(1 + \beta \int_0^t \left|f_{pto}(t)\right| dt\right), \tag{10}$$

where β is a constant, dependent on the PTO characteristics, reflecting the inherent degradation sensitivity of the PTO to the control signal.

Therefore, PTO reliability is obtained by substituting (10) into (8) as:

$$\begin{aligned} R(t) &= e^{-\int_0^t \lambda_0\left(1+\beta\int_0^t \left|f_{pto}(t)\right|dt\right)dt} \\ &= e^{-\lambda_0 t} e^{-\lambda_0\beta\int_0^t(\int_0^t |f_{pto}(t)|dt)dt} \\ &= e^{-\lambda_0 t} R_{var}(f_{pto}(t)) \\ &= R_{nom}(t)R_{var}(f_{pto}(t)), \end{aligned} \tag{11}$$

where R_{nom} and $R_{var}(f_{pto}(t))$ are the nominal and control-dependant parts of R, respectively. Now, $\boldsymbol{B_1}(t)$ can be modelled as a loss of PTO effectiveness [35]:

$$\boldsymbol{B_1}(t) = -R(t)\boldsymbol{B_2}. \tag{12}$$

Remark 2: It is worth noting that the main reliability function parameters in (11) are β and λ_0. Considering failure data scarcity in the wave energy sector, λ_0 could be approximated based on nominal failure rates of similar PTOs in other applications [45]. Moreover, the reliability function is not restricted to a specific PTO type. The reliability function can be extended to different PTO types, with the main modifications arising in the reliability-model parameters, such as λ_0 and β.

2) RELIABILITY-AWARE WEC STATE-SPACE MODEL

Considering (11), (12) and **Definition** 2, the state-space model for a degrading WEC, similar to (7), can be written as:

$$\begin{cases} \dot{\boldsymbol{x}}(t) = \boldsymbol{A}\boldsymbol{x}(t) + \boldsymbol{B_1}(t)f_{pto}(t) + \boldsymbol{B_2}f_{ex}(t), \\ y_v(t) = \boldsymbol{C_v}\boldsymbol{x}(t), \quad y_z(t) = \boldsymbol{C_z}x(t), \\ \boldsymbol{B_1}(t) = R(t)\boldsymbol{B_1} = -R(t)\boldsymbol{B_2}. \end{cases} \tag{13}$$

Throughout this paper, the following assumption is considered for $0 < R(f_{pto}(t)) \leqslant 1$:

Assumption 1:

1) The pair $(\boldsymbol{A_d}, \boldsymbol{B_1}(t))$ is stabilisable.
2) Full state information of $\boldsymbol{x(t)}$ is available.
3) The undisturbed system, $\dot{\boldsymbol{x}}(t) = \boldsymbol{A}\boldsymbol{x}(t) + \boldsymbol{B_1}(t)f_{pto}(t)$, is (strictly) dissipative [46].

III. HEALTH-AWARE CONTROLLER DESIGN

To develop a health-aware control law, the optimisation problem, depicted in Fig. 2, is written as:

$$\begin{cases} \max_{f_{pto}(t)} J = \underbrace{E_c\left(f_{pto}(t)\right)}_{\text{Actual Energy Term}} + q \underbrace{\chi\left(f_{pto}(t)\right)}_{\text{Health-Aware Penalty}}, \\ E_c(t) = \int_0^T f_{pto}(t)x_2(t)\,dt. \end{cases} \tag{14}$$

In (14), $E_c(t)$ represents the actual energy absorbed by the degrading PTO (i.e., $\boldsymbol{B_1}(t) = R(t)\boldsymbol{B_1}$), and $\chi(f_{pto}(t))$ quantifies the expected degradation cost based on the control effort. Note that absorbed *mechanical* energy at the PTO interface (rather than electrical energy [47], [48]) is considered in this paper since the focus of this work is on mechanical PTO degradation, while electrical components, including the generator and power converter, are generally more resilient, provided they are operated within their specifications.

Considering the lifetime metric (i.e., $\chi(f_{pto}(t))$) in (14), $\chi(f_{pto}(t))$ can be defined as a term, including the reliability function ($R(t)$), in (11), as:

$$\chi(f_{pto}(t)) = \int_0^{\mathsf{T}} R(t)[f_{pto}(t)]^2 dt. \tag{15}$$

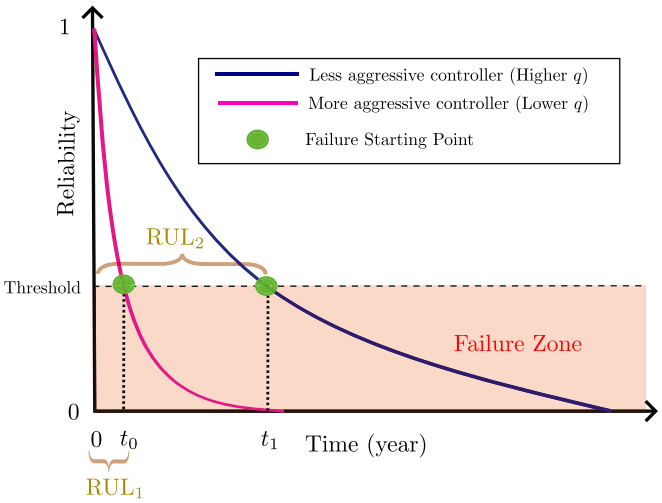

FIGURE 5. Illustration of reliability and remaining useful life (RUL) relationship. Inspired by [34].

Utilising (15), the single-objective optimisation problem, in Fig. 2, can now be represented as follows:

$$\max_{f_{pto}(t)} J = \int_0^{\mathsf{T}} f_{pto}(t)x_2(t) + qR(t)[f_{pto}(t)]^2)dt, \qquad (16)$$

$$\text{s.t.} \begin{cases} |x_1(t)| \le x_1^{\max}, \\ |x_2(t)| \le x_2^{\max}, \\ |f_{pto}(t)| \le f_{pto}^{\max}, \\ \text{the system model in (13)}, \end{cases}$$

where q is a scalar, showing a trade-off between the lifetime metric, i.e. reliability, and captured energy. $x_1^{\max}$, $x_2^{\max}$ and $f_{pto}^{\max}$ are positive scalars representing maximum displacement, velocity, and control input values, respectively.

Remark 3: It is worth mentioning that the embedding of a quadratic control effort term as a proxy for degradation in (16) (that is, $\chi(t) = \int_0^{\mathsf{T}} R(t)[f_{pto}(t)]^2 dt$) is a common practice in the health-aware control literature [40], [44].

Remark 4: If sufficient failure data is available, failure thresholds of components can be estimated by Bayesian estimation techniques, such as particle filters [49]. However, considering the paucity of failure data in the wave energy sector, estimating failure thresholds for WEC components is challenging. Nevertheless, the proposed health-aware controller can globally increase the remaining useful life (RUL) of the PTO, independently of failure threshold values (see, for example, Fig. 5). In Section IV, due to the unavailability of failure thresholds, mean time to failure (MTTF) is used to interpret reliability graphs instead of RUL. MTTF is defined as the expectation value (i.e., $\mathbb{E}(.)$) of RUL from $t = 0$ [34] :

$$MTTF = \mathbb{E}(RUL(0)) = \int_0^{\infty} R(t)dt. \qquad (17)$$

Remark 5: While the formulation in (16) may superficially resemble a PTO (actuator) mismatch control problem, which is commonly addressed in the robust control literature [50], the key distinction here lies in how the loss of PTO effectiveness is modelled. In this paper, the loss of PTO effectiveness is not treated as an uncertainty or mismatch, but rather as the component health metric (i.e., reliability), aligning with the concept of health-aware control, where the component health status is used in the controller design [21].

Remark 6 (PTO losses versus PTO reliability): PTO losses and PTO reliability describe different phenomena. PTO losses quantify inefficiencies in converting absorbed mechanical power to delivered electrical power [48], whereas reliability characterises the probability of failure (i.e., loss of the ability to perform the required function) and is commonly modelled through a failure rate [36]. Accordingly, a loss model is not, in general, a direct substitute for a reliability model, since PTO losses can arise even when the PTO is healthy. In this paper, the proposed health-aware EMPC is reliability-aware rather than loss-aware, i.e., the controller explicitly trades absorbed mechanical energy against a probabilistic lifetime metric (reliability). If desired, PTO losses could be incorporated by augmenting the performance objective with an additional loss proxy term (e.g., a function of f_{pto} (control force) and x_2 (velocity) as in [48]); however, this extension is not pursued here.

A. RELIABILITY-AWARE ECONOMIC MODEL PREDICTIVE CONTROL FRAMEWORK

To transform the single-objective optimisation problem, in (16), into a regular EMPC formulation [51], two steps need to be performed:

1) Converting maximisation problem (16) to a minimisation problem as:

$$\min_{f_{pto}(k)} J_d = \sum_{k=0}^{N-1} -x_2(k)f_{pto}(k) + \frac{q}{R(k)}[f_{pto}(k)]^2, \quad (18)$$

where N is the prediction horizon. Note that the inversion of $R(k)$ arises from converting the maximisation problem into a minimisation form, which ensures that small reliability values (i.e., higher degradation) result in larger penalties on the control input, preserving the intended health-aware objective in (16).

2) Discretising WEC model (13) as:

$$\begin{cases} \boldsymbol{x(k+1)} = \boldsymbol{A_d x}(k) + \boldsymbol{B_{1d}}(k)f_{pto}(k) + \boldsymbol{B_{2d}}f_{ex}(k), \\ y_v(k) = \boldsymbol{C_v x}(k), \quad y_z(k) = \boldsymbol{C_z}x(k), \\ \boldsymbol{B_{1d}}(k) = -R(k)\boldsymbol{B_{2d}}. \end{cases} \qquad (19)$$

where $\boldsymbol{A_d}, \boldsymbol{B_{1d}}(k)$, and $\boldsymbol{B_{2d}}$ are discrete version of $\boldsymbol{A}, \boldsymbol{B_1}(t)$, and $\boldsymbol{B_2}$.

Remark 7: $R(k)$ in the performance function (18) varies slowly over time within the prediction horizon. Therefore, to maintain convexity and computational efficiency during real-time optimisation, it is reasonable to treat $R(k)$ as a constant scalar within the prediction horizon, set to its current value, that is, $R(k) \approx R(0|k)$; as a result, $\boldsymbol{B_{1d}}(0|k) = -R(0|k)\boldsymbol{B_{2d}}$.

Similarly, it is reasonable to estimate the system, in (19), with the following model over the prediction horizon (i.e., N) as:

$$\begin{cases} \boldsymbol{x(k+1)} = \boldsymbol{A_d x}(k) + \boldsymbol{B_{1d}}(0|k) f_{pto}(k) + \boldsymbol{B_{2d}} f_{ex}(k), \\ y_v(k) = \boldsymbol{C_v x}(k), \quad y_z(k) = \boldsymbol{C_z} x(k), \\ \boldsymbol{B_{1d}}(0|k) = -R(0|k)\boldsymbol{B_{2d}}. \end{cases} \tag{20}$$

Remark 8: Recent studies in EMPC [28], [52], [53] show that when the stage cost is economic, appending a terminal cost based on the state vector can guarantee closed-loop stability. Therefore, similarly, the following state-based terminal cost is considered in this paper:

$$V_f(\boldsymbol{x}(N)) = \boldsymbol{x}^\intercal(N)\boldsymbol{P}\boldsymbol{x}(N).$$

Therefore, a health-aware EMPC control problem, considering **Remark** 7, **Remark** 2 and (18), can be written as:

$$\begin{aligned} \min_{f_{pto}(k)} J_d = V_f(\boldsymbol{x}(N)) + \sum_{k=0}^{N-1} -x_2(k) f_{pto}(k) \\ + \frac{q}{R(0|k)}[f_{pto}(k)]^2 \end{aligned} \tag{21}$$

$$\text{s.t.} \begin{cases} |x_1(k)| \le x_1^{\max}, \\ |x_2(k)| \le x_2^{\max}, \\ |f_{pto}(k)| \le f_{pto}^{\max}, \\ \text{the system model in (20).} \end{cases}$$

1) UNCONSTRAINED QUADRATIC PROGRAMMING FORMULATION

To develop a QP formulation for the EMPC in (21), prediction vectors up to $N-1$ steps ahead for the velocity output ($y_v(k)$), control input ($f_{pto}(k)$), wave excitation force ($f_{ex}(k)$) are written as:

$$\begin{cases} \boldsymbol{F_{pto}} = [f_{pto}(k), f_{pto}(k+1|k) \cdots f_{pto}(k+N-1|k)]^\intercal, \\ \boldsymbol{Y_v} = [y_v(k), y_v(k+1|k) \cdots y_v(k+N-1|k)]^\intercal, \\ \boldsymbol{F_{ex}} = [f_{ex}(k), f_{ex}(k+1|k), \cdots f_{ex}(k+N-1|k)]^\intercal, \end{cases} \tag{22}$$

where $f_{pto}(k+i|k)$, $y_v(k+i|k)$, and $f_{ex}(k+i|k)$ for $i \in \{1, 2, \ldots, N-1\}$ are predicted values of $f_{pto}(k+i)$, $y_v(k+i)$, and $f_{ex}(k+i)$ at time k, respectively. Noting that $y_v = \boldsymbol{C_v} x = x_2$, the objective function, in (21), can be rewritten as:

$$\begin{aligned} J_d := & -\boldsymbol{F_{pto}^\intercal Y_v} \\ & + \boldsymbol{F_{pto}^\intercal} \left(\frac{\boldsymbol{1}}{\boldsymbol{R(0|k)}} \begin{bmatrix} \boldsymbol{q} & \boldsymbol{0} & \cdots & \boldsymbol{0} \\ \boldsymbol{0} & \boldsymbol{q} & \cdots & \boldsymbol{0} \\ \vdots & \vdots & \ddots & \vdots \\ \boldsymbol{0} & \boldsymbol{0} & \cdots & \boldsymbol{q} \end{bmatrix} \right) \boldsymbol{F_{pto}} + V_f(\boldsymbol{x}(N)) \end{aligned}$$

Then, similar to [13], [54], $\boldsymbol{Y_v}$ can be represented by propagating y_v, in (20), as:

$$\boldsymbol{Y_v} = \boldsymbol{\Lambda_1 x} + \boldsymbol{\Phi_{F_{pto1}} F_{pto}} + \boldsymbol{\Phi_{D1} F_{ex}}, \tag{23}$$

where

$$\begin{cases} \boldsymbol{\Lambda_1} = \begin{bmatrix} \boldsymbol{C_v} & \boldsymbol{C_v A_d} & \boldsymbol{C_v A_d^2} & \cdots & \boldsymbol{C_v A_d^N} \end{bmatrix}^\intercal \\ \boldsymbol{\Phi}_{\mathrm{F_{pto1}}} = -R(0|k) \times \boldsymbol{\Phi}_{\mathrm{D_1}} \\ \boldsymbol{\Phi}_{\mathrm{D_1}} \\ = \begin{bmatrix} \boldsymbol{0} & & & & \\ \boldsymbol{C_v B_{2d}} & \boldsymbol{0} & & & \\ \boldsymbol{C_v A_d B_{2d}} & \boldsymbol{C_v B_{2d}} & \boldsymbol{0} & & \\ \vdots & \vdots & \ddots & \ddots & \\ \boldsymbol{C_v A_d^{N-1} B_{2d}} & \boldsymbol{C_v A_d^{N-2} B_{2d}} & \cdots & \boldsymbol{C_v B_{2d}} & \boldsymbol{0} \end{bmatrix}. \end{cases}$$

Substituting (23) into (21) results in the following unconstrained QP optimisation problem:

$$\min_{\boldsymbol{F_{pto}}} J_d = \frac{1}{2} \boldsymbol{F_{pto}^\intercal \mathcal{H} F_{pto}} + \boldsymbol{\mathcal{F}^\intercal F_{pto}}, \tag{24}$$

$$\text{s.t.} \begin{cases} \boldsymbol{x(k+1)} = \boldsymbol{A_d x}(k) + \boldsymbol{B_{1d}}(0|k) f_{pto}(k) + \boldsymbol{B_{2d}} f_{ex}(k), \\ y_v(k) = \boldsymbol{C_v x}(k), \quad y_z(k) = \boldsymbol{C_z} x(k), \\ \boldsymbol{B_{1d}}(0|k) = -R(0|k)\boldsymbol{B_{2d}}. \end{cases}$$

with $\boldsymbol{\mathcal{H}}$ and $\boldsymbol{\mathcal{F}}$ as:

$$\begin{cases} \boldsymbol{\mathcal{H}} = -\boldsymbol{\Phi_{F_{pto1}}} - \boldsymbol{\Phi_{F_{pto1}}^\intercal} \\ \quad + \frac{2}{R(0|k)} \begin{bmatrix} q & 0 & \cdots & 0 \\ 0 & q & \cdots & 0 \\ \vdots & \vdots & \ddots & \vdots \\ 0 & 0 & \cdots & q \end{bmatrix} + 2\boldsymbol{\Phi_{F_{ptoN}}^\intercal P \Phi_{F_{ptoN}}}, \\ \boldsymbol{\mathcal{F}} = -\boldsymbol{\Lambda_1 x}(k) - \boldsymbol{\Phi_{D1} F_{ex}} \\ \quad + \boldsymbol{\Phi_{F_{ptoN}}^\intercal P} \left(\boldsymbol{\Lambda_N x(k) + \Phi_{DN} F_{ex}} \right). \end{cases}$$

where

$$\begin{cases} \boldsymbol{\Lambda_N} = \boldsymbol{A_d^N}, \\ \boldsymbol{\Phi_{F_{ptoN}}} = -R(0|k)\boldsymbol{\Phi_{DN}}, \\ \boldsymbol{\Phi_{DN}} = \begin{bmatrix} \boldsymbol{A_d^{N-1} B_{2d}} \cdots \boldsymbol{A_d B_{2d}} \boldsymbol{B_{2d}} \end{bmatrix}. \end{cases}$$

2) CONSTRAINED QUADRATIC PROGRAMMING FORMULATION

For the constrained QP optimisation problem, the predicted position output (i.e., $\boldsymbol{Y_z}$) is defined, since $\boldsymbol{Y_z}$ is required to obtain the QP formulation of the position constraint. So, $\boldsymbol{Y_z}$, similarly to $\boldsymbol{Y_v}$, in (23), is written as:

$$\boldsymbol{Y_z} = \boldsymbol{\Lambda_2 x} + \boldsymbol{\Phi_{F_{pto2}} F_{pto}} + \boldsymbol{\Phi_{D2} F_{ex}}, \tag{25}$$

where $\boldsymbol{\Lambda_2}$, $\boldsymbol{\Phi_{D2}}$ and $\boldsymbol{\Phi}_{\mathrm{F_{pto2}}}$ are defined in the same manner as $\boldsymbol{\Lambda_1}$, $\boldsymbol{\Phi_{D1}}$ and $\boldsymbol{\Phi}_{\mathrm{F_{pto1}}}$ in (23), but $\boldsymbol{C_z}$ is used instead of $\boldsymbol{C_v}$. Therefore, the physical constraints, in (21), can be rewritten as:

$$\boldsymbol{A_{con} F_{pto}} \leqslant \boldsymbol{b_{con}}, \tag{26}$$

where

$$\begin{cases} \boldsymbol{A_{con}} = \begin{bmatrix} \boldsymbol{I} \\ -\boldsymbol{I} \\ \boldsymbol{\Phi}_{\boldsymbol{F_{pto2}}} \\ -\boldsymbol{\Phi}_{\boldsymbol{F_{pto2}}} \\ \boldsymbol{\Phi}_{\boldsymbol{F_{pto1}}} \\ -\boldsymbol{\Phi}_{\boldsymbol{F_{pto1}}} \end{bmatrix}, \\ \boldsymbol{b_{con}} = \begin{bmatrix} f_{pto}^{\max}\mathbf{1}_{(N+1)\times 1} \\ f_{pto}^{\max}\mathbf{1}_{(N+1)\times 1} \\ x_1^{\max}\mathbf{1} - \boldsymbol{\Lambda_2 x}(k) - \boldsymbol{\Phi_{D2}F_{ex}} \\ x_1^{\max}\mathbf{1} + \boldsymbol{\Lambda_2 x}(k) + \boldsymbol{\Phi_{D2}F_{ex}} \\ x_2^{\max}\mathbf{1} - \boldsymbol{\Lambda_1 x}(k) - \boldsymbol{\Phi_{D1}F_{ex}} \\ x_2^{\max}\mathbf{1} + \boldsymbol{\Lambda_1 x}(k) + \boldsymbol{\Phi_{D1}F_{ex}} \end{bmatrix}, \\ \mathbf{1} = [\underbrace{1, \ldots, 1}_{N+1}]^\intercal, \\ \boldsymbol{I} = \begin{bmatrix} 1 & 0 & \cdots & 0 \\ 0 & 1 & \cdots & 0 \\ \vdots & \vdots & \ddots & \vdots \\ 0 & 0 & \cdots & 1 \end{bmatrix}_{(N+1)\times(N+1)}. \end{cases}$$

Now, the constrained QP optimisation problem, considering (24) and (26), can be proposed as:

$$\min_{\boldsymbol{F_{pto}}} J_d = \frac{1}{2}\boldsymbol{F_{pto}^\intercal \mathcal{H} F_{pto}} + \boldsymbol{\mathcal{F}^\intercal F_{pto}}, \tag{27}$$

$$\text{s.t.} \begin{cases} \boldsymbol{x(k+1)} = \boldsymbol{A_d x}(k) + \boldsymbol{B_{1d}}(0|k) f_{pto}(k) + \boldsymbol{B_{2d}} f_{ex}(k), \\ y_v(k) = \boldsymbol{C_v x}(k), \quad y_z(k) = \boldsymbol{C_z} x(k), \\ \boldsymbol{B_{1d}}(0|k) = -R(0|k)\boldsymbol{B_{2d}}, \\ \boldsymbol{A_{con}F_{pto}} \leqslant \boldsymbol{b_{con}}. \end{cases}$$

Theorem 1: Considering **Assumption** 1, the proposed health-aware EMPC, for the WEC model (19), guarantees the closed-loop Input-to-state (ISS) Lyapunov stability [55], where the terminal cost $\boldsymbol{P}_j$ matrix, for every horizon $j \in \{1, 2, \ldots, \infty\}$, is the solution of the following discrete Riccati equation:

$$\begin{aligned} \boldsymbol{P}_j = \boldsymbol{A_d^\intercal P_j A_d} - \left(\boldsymbol{S} + \boldsymbol{B_{1dj}^\intercal P_j A_d}\right)^\intercal \\ \times \left(\boldsymbol{r_j} + \boldsymbol{B_{1d}^\intercal P_j B_{1dj}}\right)^{-1} \left(\boldsymbol{S} + \boldsymbol{B_{1dj}^\intercal P_j A_d}\right), \end{aligned} \tag{28}$$

where $\boldsymbol{S} = [0, -1, \mathbf{0}_{n_r\times 1}]$, $r_j = \frac{q}{R_j(0|k)}$ and $\boldsymbol{B_{1dj}} = -R_j(0|k)\boldsymbol{B_{2d}}$.

Proof: See **Appendix** A. ■

IV. HEALTH-AWARE CONTROL RESULTS

In this section, health-aware control results are presented. First, model setup and simulation parameters are presented in Section IV-A. Then, the effect of β on the reliability function is investigated in Section IV-B, and the constraint-handling performance of the proposed health-aware controller for a specific β and q is investigated in Section IV-C. Finally, Section IV-D explores the effect of q in the trade-off between captured energy and PTO lifetime.

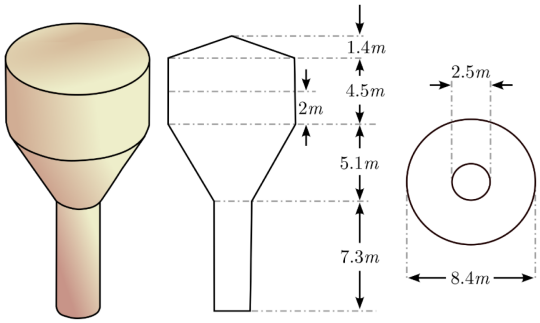

FIGURE 6. Schematic illustration of the point absorber WEC device in the current study [58].

TABLE 1. Simulation parameters.

WEC	
Total mass	1.4706×10^5 [kg]
Hydrostatic stiffness s_h	5.57×10^5 [N/m]
Radiation subsystem dimension n_r	6
Discretisation method	First-order hold
Physical constraints	
Maximum position x_1^{max}	2 [m]
Maximum velocity x_2^{max}	2 [m/s]
Maximum control input f_{pto}^{max}	1×10^6 [N]
EMPC parameters	
Sampling interval T_s	0.1 [s]
Prediction horizon N	80 steps
Trade-off parameter q	7×10^{-7}
Optimisation algorithm	MATLAB-quadprog
PTO reliability parameters	
λ_0 (Direct drive PTO [45])	0.93 [failures/year]

A. MODEL SETUP AND SIMULATION PARAMETERS

The current study employs a heaving point absorber WEC, depicted in Fig. 6, along with its dimensions. This study considers irregular waves, which are stochastically generated from a JONSWAP spectrum [56]. These waves are characterised with $H_s = 2.5$ m, $T_p = 10.5$ s, and $\gamma = 3.3$, representing the most common sea state at the Atlantic Marine Energy Test Site (AMETS), Berth A, off the north-west coast of Ireland [57]. The remaining simulation parameters are detailed in Table 1. It should be noted that the current article assumes perfect knowledge of the wave excitation force. Although it is more realistic to consider a non-ideal forecaster with the proposed health-aware EMPC, due to the immeasurable nature of the wave excitation force, an ideal forecaster is considered for the sake of simplicity, focussing on the main contribution, i.e. the first optimisation-based health-aware WEC controller in the wave energy literature. In addition, this assumption does not affect the ability of health-aware EMPC to adjust a trade-off between captured energy and lifetime.

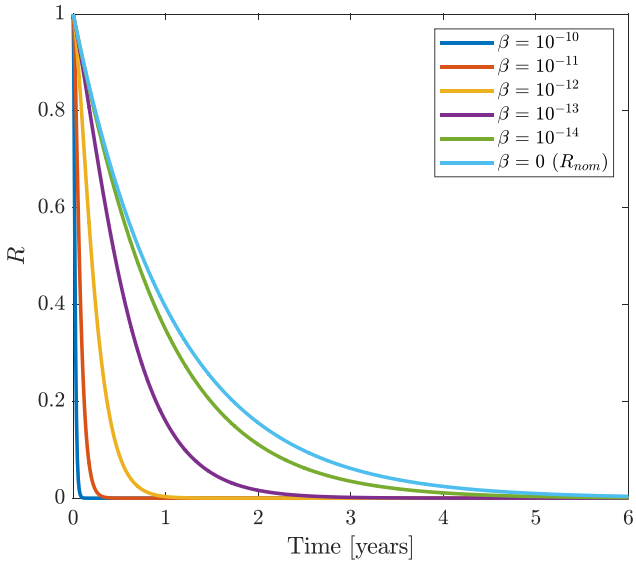

FIGURE 7. Effect of β variations on PTO reliability for the test control input in (30).

Remark 9: Please note that all energy and power plots are based on the degrading PTO as:

$$\begin{cases} E_c(t) = \int_0^T f_{pto}(t)x_2(t)dt, \\ \dot{\boldsymbol{x}}(t) = \boldsymbol{A}\boldsymbol{x}(t) + \boldsymbol{B_1}(t)f_{pto}(t) + \boldsymbol{B_2}f_{ex}(t). \end{cases} \tag{29}$$

B. IMPACT OF β VARIATION ON THE RELIABILITY FUNCTION

In this section, the effect of parameter β on PTO degradation is studied. In recent WEC reliability studies [45], [59], [60], the main focus is on how to estimate the nominal failure rate λ_0 of components, based on nominal failure rates of similar components in other industries, such as oil and gas. Therefore, calculating β parameters for WEC components, such as PTO, is an open discussion. For a test control signal

$$f_{pto}(t) = f_{pto}^{\max}(t)sin\left(\frac{2\pi t}{6}\right), \tag{30}$$

the reliability function, in (11), can be computed for different values of β, as depicted in Fig. 7. The curves represent the effect of varying β from 10^{-10} to 0, specifying the decay rate of the reliability function. As β decreases, the decay rate slows down, leading to a more gradual decrease in reliability over time. The light blue solid line (i.e., $\beta = 0$) exhibits the slowest decay. In contrast, the blue solid line (i,e, $\beta = 10^{-10}$) shows the fastest decay, indicating that larger values of β result in more rapid declines in reliability. Table 2 shows the effect of β on the MTTF of the PTO. Table 2 shows that, as β decreases from 10^{-10} to 0, the MTTF increases, indicating a longer lifetime. Specifically, for $\beta = 10^{-10}$, the MTTF is 0.0351 years, progressively increasing to 1.0753 years when $\beta = 0$. This trend suggests that smaller values of β result in a more reliable system with a higher MTTF. Based on the simulation results presented in this section, a value of $\beta = 10^{-13}$ is selected in Sections IV-C and IV-D to provide a balanced evaluation of PTO degradation, neither overly sensitive nor insensitive to the control input.

TABLE 2. MTTF for different β for the test control input in (30), the chosen β is highlighted in yellow.

Parameter	Value					
β	10^{-10}	10^{-11}	10^{-12}	10^{-13}	10^{-14}	0
MTTF [year]	0.0351	0.0654	0.2781	0.6253	0.9533	1.0753

C. PERFORMANCE OF CONSTRAINED AND UNCONSTRAINED HEALTH-AWARE EMPC

In this section, the performance of the unconstrained and constrained EMPCs, proposed in Section III, in terms of constraints handling, is discussed to show the proposed controller has the same constraint handling ability as typical MPC or MPC-like energy-maximising WEC controllers have. However, in Section IV-D, the lifetime enhancement characteristic of the proposed controller is also fully discussed.

In particular, Fig. 8 displays the position, velocity, and control input over time, for both unconstrained and constrained EMPC cases. The grey dashed line represents the unconstrained EMPC, while the black solid line represents the constrained EMPC. The position (z) and velocity ($\dot{z}$) graphs show that the unconstrained EMPC has a more exaggerated state response than the constrained EMPC. The control input ($f_{pto}(t)$) graph, as expected, shows the unconstrained EMPC has larger magnitudes. The dashed red lines represent the constraints for position, velocity, and control input, demonstrating that the constrained EMPC is able to handle both state and control input constraints effectively.

Fig. 9 illustrates the average absorbed power for the constrained EMPC, for various peak wave periods (T_p). For this particular result, 20 realisations of each sea state were considered, with each realization lasting 200 times the peak period to get statistically consistent results [61]. It can be seen that the average power changes significantly as T_p increases from 5 s to 8 s, whereas for larger values of T_p the variation in average power is much smaller.

D. IMPACT OF q VARIATION ON CONTROL PERFORMANCE

The current section investigates how the proposed health-aware controller provides a means to specify a trade-off between captured energy and PTO lifetime. In the current section, results are extrapolated, based on four-day simulated data, since simulating the proposed EMPC over years is computationally expensive, and provides little additional resolution. Energy plots, in Fig. 10, are extrapolated using integration of exponential functions, considering the nonlinear behaviour of energy due to reliability (i.e., $\int_0^T f_{pto}(t)x_2(t)dt$). Similarly, reliability plots, in Fig. 11, are extrapolated using exponential functions, due to their exponential nature, as shown in Section IV-B. In particular, Fig. 10 highlights

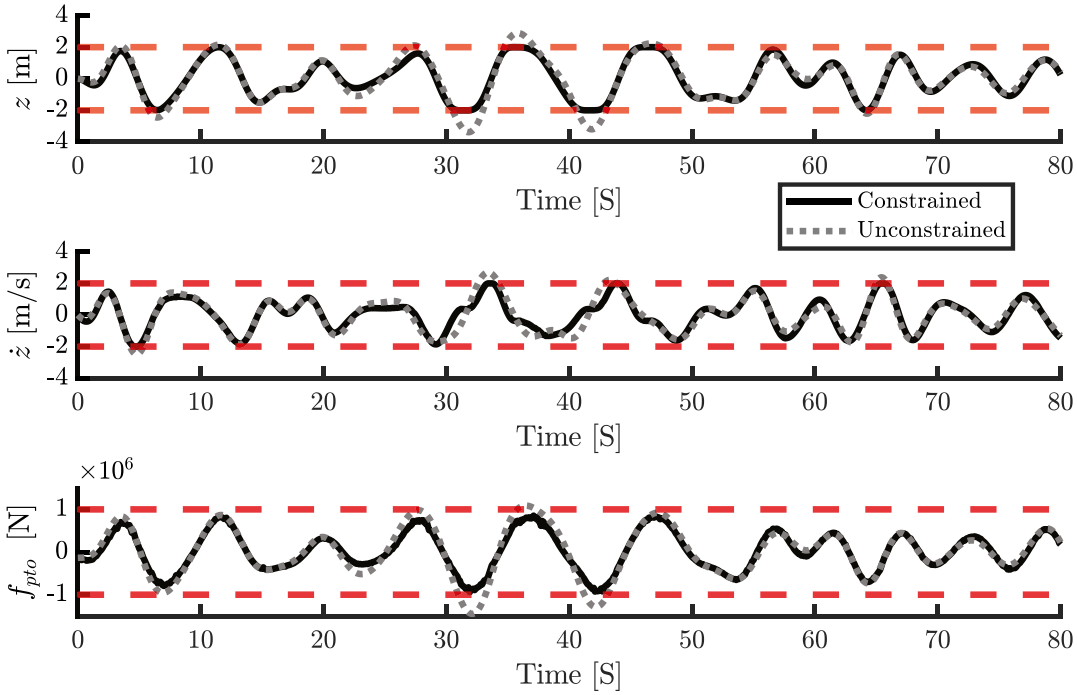

FIGURE 8. WEC position [m] (z), velocity [m/s] ($\dot{z}$) and control input ($f_{pto}(t)$) [N] for the unconstrainted EMPC (grey dashed line) and constrained EMPC (black solid line) with $q = 7 \times 10^{-7}$ and $\beta = 10^{-13}$, under irregular ocean waves with $T_p = 10.5$ [s] and $H_s = 2.5$ [m]; The dashed red lines represent position, velocity, and control input constraints.

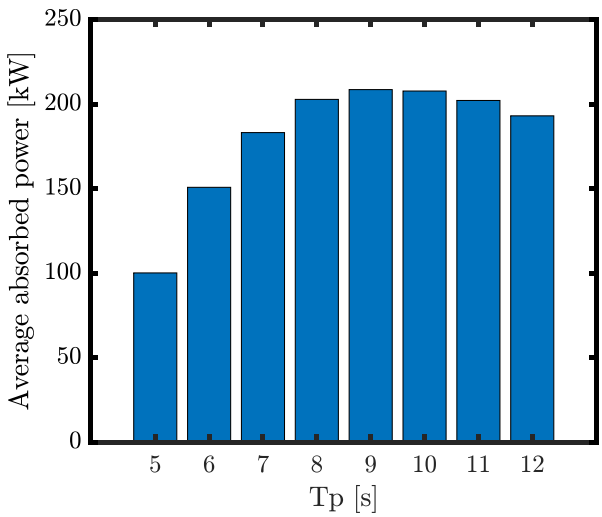

FIGURE 9. Average absorbed power for the constrained EMPC, with $q = 7 \times 10^{-7}$ and $\beta = 10^{-13}$, under irregular ocean waves with $H_s = 2.5$ [m] and various T_p.

the extrapolated energy graph for various values of q, under constrained and unconstrained EMPC with $\beta = 10^{-13}$. It can be seen, from Fig. 10, that the energy increases over time, with a more aggressive increase associated with smaller values of q, indicating that the health-aware EMPC focuses less on lifetime. The constrained EMPC tends to result in less absorbed energy, compared to the unconstrained case, which is a testimony of the limiting motion of the system under constrained EMPC. To complement the extrapolation results, Fig. 12 shows representative 80 s time histories of z, $\dot{z}$, and f_{pto} at three degradation levels corresponding to a healthy PTO ($R \approx 1$), a one-year degraded PTO ($R \approx 0.28$), and a severely degraded five-year PTO ($R \approx 10^{-4}$). For a fair comparison, the controller parameters are kept fixed ($q = 7 \times 10^{-7}$, $\beta = 10^{-13}$), and the same irregular sea state realisation is used ($T_p = 10.5$ s, $H_s = 2.5$ m). As R decreases, the achievable PTO force decreases, thereby reducing the motion response.

Fig. 11 presents the extrapolated reliability graphs, for different values of q, using four-day of simulation data, with $\beta = 10^{-13}$. Fig. 11 shows that, as q decreases, the slope of the reliability curves increases more intensely, particularly for the unconstrained case. The curve corresponding to $q = 0$ grows most rapidly, indicating that the smaller the value of q, the lower is the consequent reliability. Interestingly, for $q = 7 \times 10^{-6}$, the unconstrained and constrained EMPCs have very similar performance, in terms of captured energy and reliability metrics, which means that a large value for q confines $f_{pto}(t)$ severely, leading to correspondingly small velocity and position variations, within the allowable bound. Fig. 13(a) and (b) present Pareto fronts that consider the variation of q, under the unconstrained and constrained EMPCs with $\beta = 10^{-13}$, respectively. The trade-off between the MTTF (i.e., lifetime) and E_c is illustrated in both Fig. 13(a) and (b). As q decreases, from 7×10^{-6} to 0, the MTTF decreases in both the constrained and unconstrained cases, with significant changes in the unconstrained case, not only in MTTF, but also in captured energy.

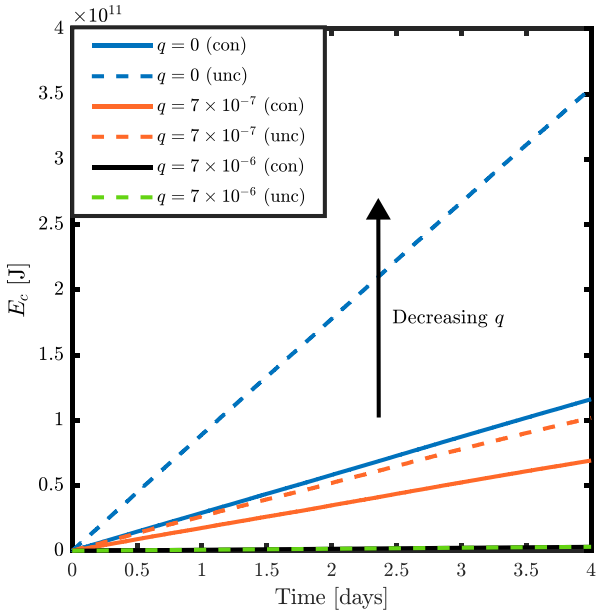

(a) Four-day simulated data

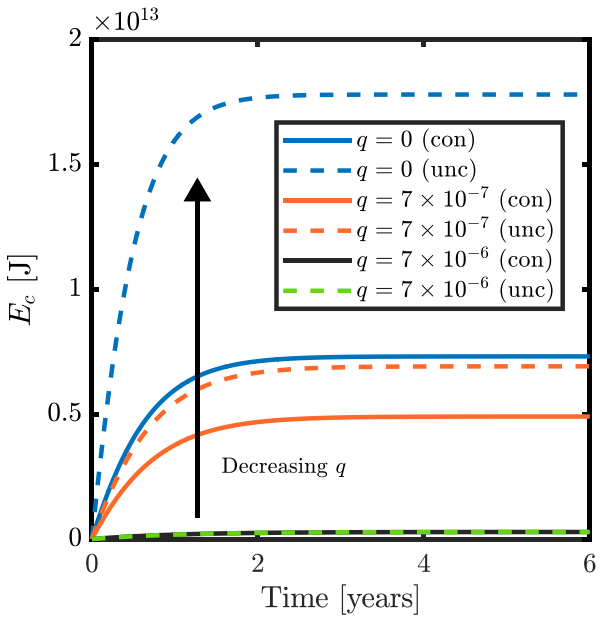

(b) Extrapolated data

FIGURE 10. Comparison of extrapolated energy graphs with different q and $\beta = 10^{-13}$ for the constrained (con) and unconstrained (unc) EMPCs. Panel (a) shows the four-day simulated data, while panel (b) presents the extrapolated data over 6 years. Results are generated under irregular ocean waves with $T_p = 10.5$ [s] and $H_s = 2.5$ [m]. The dashed arrows indicate the trend of decreasing values of q, for both constrained and unconstrained cases.

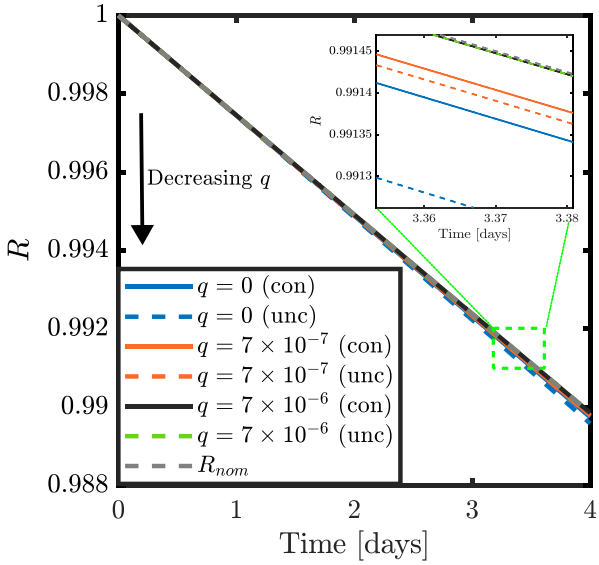

(a) Four-day simulated data

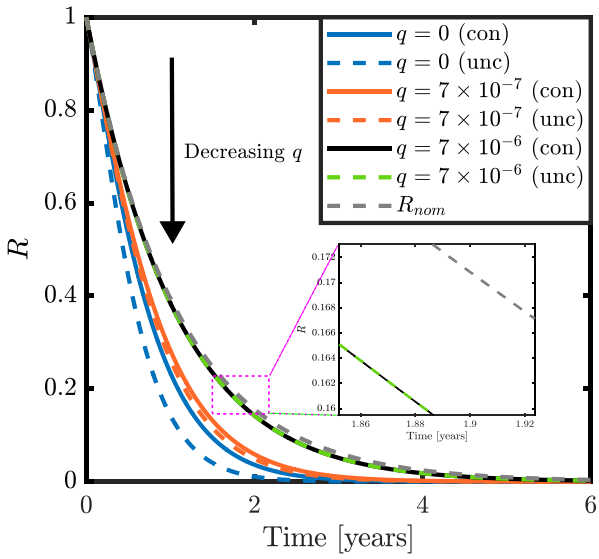

(b) Extrapolated data

FIGURE 11. Comparison of extrapolated reliability graphs with different q and $\beta = 10^{-13}$ for the constrained (con) and unconstrained (unc) EMPCs. Panel (a) shows the four-day simulated data, while panel (b) presents the extrapolated data over 6 years. Results are generated under irregular ocean waves with $T_p = 10.5$ [s] and $H_s = 2.5$ [m]. The dashed arrows indicate the trend of decreasing values of q, for both constrained and unconstrained cases.

Remark 10: Note that when q converges to zero, the proposed optimisation problem in (21) progressively becomes nonconvex, aligning with the results of energy-maximising EMPC studies, e.g. [13], [27], [28], which consider additional terms in the performance function. Precisely, in the unconstrained case, the optimisation problem in (24) is non-convex with $q = 0$. Therefore, in this case, to get a convex solution, it is assumed that $|f_{pto}(t)| < 2.5 \times 10^6$ which is beyond, the actual control input limit of $|f_{pto}(t)| < 1 \times 10^6$ in Table 1.

It should be noted that maximum WEC lifetime is typically considered as 20 years [62]; however, based on Fig. 13(b), the PTO fails in less than 13 months. The reason is that the reliability metric considers component lifetime without any maintenance [36]. Therefore, health-aware EMPC aims to increase lifetime by delaying maintenance until a later

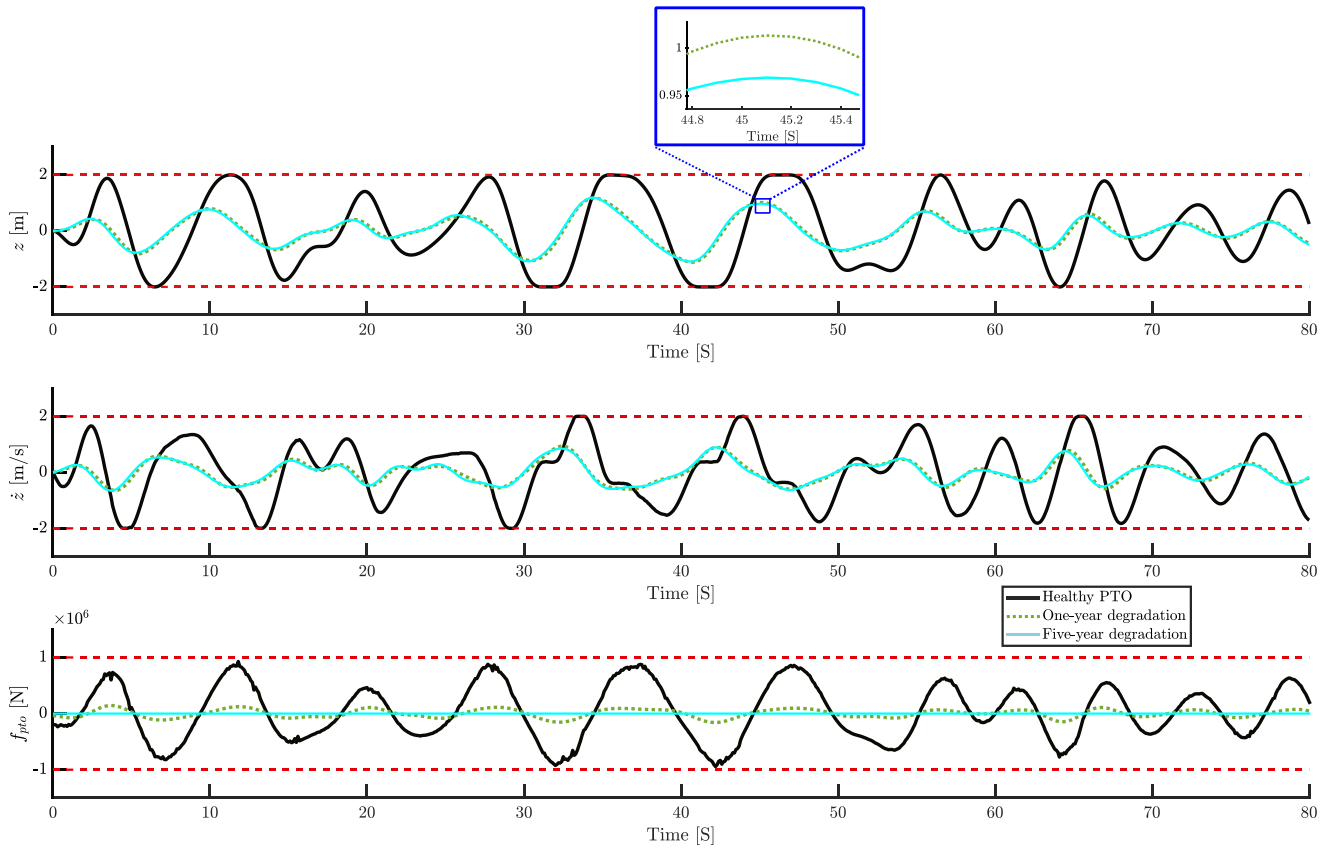

FIGURE 12. Comparison of representative time histories of position z, velocity $\dot{z}$, and PTO force f_{pto} for three degradation levels using fixed controller tuning ($q = 7 \times 10^{-7}$, $\beta = 10^{-13}$): healthy PTO ($R \approx 1$, solid black), one-year degraded PTO ($R \approx 0.28$, dotted green), and five-year degraded PTO ($R \approx 10^{-4}$, solid light blue). Dashed red lines indicate the position, velocity, and control-force constraints. Results are shown for the same irregular sea state realisation ($T_p = 10.5$ s, $H_s = 2.5$ m).

time. For example, consider a constrained energy-maximising EMPC (i.e., $q = 0$), used with a yearly fixed maintenance interval. Based on Fig. 13(b), the MTTF value for such a controller is ≈ 8.5 months, meaning that there is no energy production for around 3.5 months after PTO failure, resulting in a relatively high LCoE. However, if $q = 7 \times 10^{-6}$is selected (health-aware policy), the PTO not only survives until the maintenance interval (MTTF $\approx$ one year), but the WEC system can absorb energy for the 3.5 months that the PTO, under the energy-maximising controller, is failing. Note that, if the system survives until the maintenance interval, there is a chance of repairing the degrading component, rather than its complete replacement, reducing OpEx. In addition, even if a 6-month maintenance interval with $q = 0$ is considered, the number of maintenance activities in 20 years is 40, while the number of maintenance activities with $q = 7 \times 10^{-6}$ with annual maintenance, is 20. Although $q = 0$ results in a significant energy increase, compared to $q = 7 \times 10^{-6}$, note that q need not be fixed at 7×10^{-6} over the full 20 years. Rather, q can be tuned dynamically between 0 and 7×10^{-6}, based on certain criteria, considering overall economic benefit, to reach a suitable trade-off between captured energy and PTO lifetime. For example, a smaller value of q may be tolerated for short period if the market price of electricity is particularly high. However, specifying such a decision criterion, and the associated decision-making algorithm, requires an explicit economic model. In particular, a full LCoE optimisation in Fig. 2 is inherently site- and device-dependent, requiring detailed information on maintenance logistics (e.g., weather windows, vessel costs, downtime, and discounting), which is beyond the scope of this control-focused paper (see, e.g., Fig. 2 in [10]). In addition, the exact mapping between the control action f_{pto} and OpEx(f_{pto}) is generally unknown.

Therefore, future work on tuning q will attempt to couple the proposed controller with a site-specific techno-economic model, which could be done via direct LCoE evaluation, enabling an economically optimal choice of q.

V. CONCLUSION

In this study, a novel health-aware WEC controller, considering PTO degradation, is studied. The proposed controller uses a novel health-aware surrogate measure of LCoE as a performance function, which includes a term (i.e., reliability) indicating the lifetime of the component (i.e., the PTO). Numerical results confirm that not only does the proposed controller handle physical constraints similarly to typical

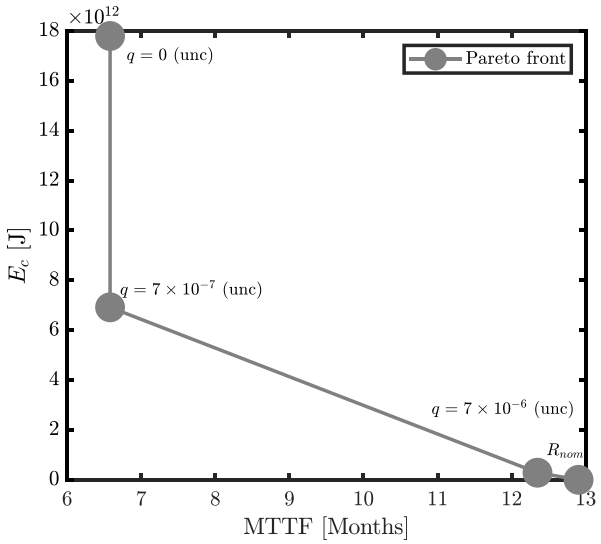

(a) Unconstrained EMPC

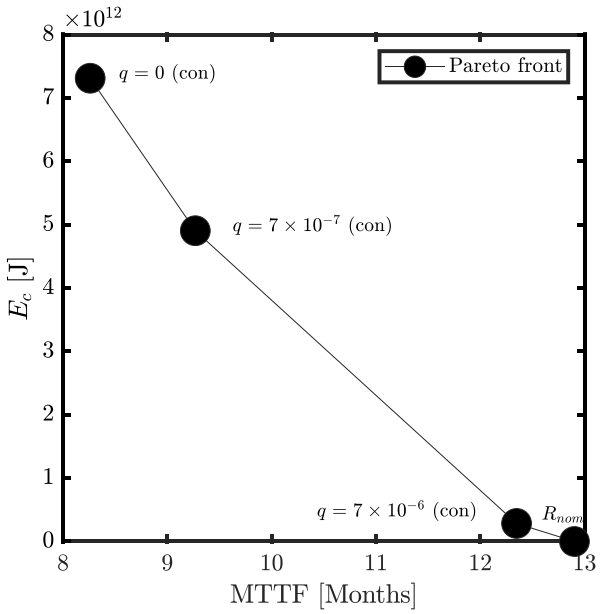

(b) Constrained EMPC

FIGURE 13. The resulting Pareto fronts considering q variations under (a) unconstrained (unc) EMPC and (b) constrained (con) EMPC with $\beta = 10^{-13}$ under irregular ocean waves with $T_p = 10.5$ [s] and $H_s = 2.5$ [m].

WEC energy-maximising controllers, but also has the unique ability to adjust a trade-off between captured energy and PTO lifetime, where larger q values result in a longer lifetime but less captured energy. One of the main challenges in health-aware control of WECs is the paucity of failure data. For the current study, this data scarcity appears as the uncertainty in reliability function parameters (i.e., β and λ_0). With access to operational control force data from a degrading PTO, the reliability metric can be estimated using the WEC model, and reliability parameters such as β and λ_0 can be identified accordingly. Such a calculation is beyond the scope of this current project, especially considering the dearth of operational WEC data available. Nevertheless, the proposed health-aware controller can globally enhance PTO lifetime irrespective of the values of λ_0 and β. In addition, numerical results show that health-aware EMPC enhances lifetime by delaying maintenance intervals. Nevertheless, the primary challenge of the health-aware controller is how q should be selected, which is crucial to adjust a lifetime-aware maintenance policy in a total 20-year WEC operation period, with further analysis required to quantify appropriate q values. However, such an analysis requires a holistic approach, that considers decision-making criteria as well as the multi-objective algorithm, to achieve the highest economic benefit and will be the subject of future research. In addition, future work will investigate an *integrated* scheme that combines real-time condition monitoring (to react to the *current* health state) with the proposed reliability-aware control (which *focuses* on shaping *future* PTO health through control-induced loading). Developing such monitoring-informed control remains challenging in the wave energy context due to the diversity of WEC/PTO technologies and the practical difficulty of instrumenting devices and estimating health reliably online. Finally, this study represents a first step toward reliability-aware WEC control; accordingly, the adopted PTO reliability model is kept simple to establish a clear baseline. Future work will extend the framework beyond the PTO to incorporate device-level structural reliability, including failure mechanisms driven by extreme external loading.

APPENDIX
PROOF OF THEOREM 1

Considering $\boldsymbol{S} = [0, -1, \mathbf{0}_{n_r \times 1}]$, $r_j = \frac{q}{R_j(0|k)}$ and $\boldsymbol{B_{1dj}} = R_j(0|k)B_{1d} = -R_j(0|k)\boldsymbol{B_{2d}}$, one can get the economic model predictive control (EMPC) problem, in (21), for every horizon, as follows:

$$\min_{f_{pto}(k)} V_{fj}(\boldsymbol{x}(N)) + \sum_{k=0}^{N-1} f_{pto}(k)\boldsymbol{S}\boldsymbol{x}(k) + r_j[f_{pto}(k)]^2, \quad \text{(A.1)}$$

$$\text{s.t.} \begin{cases} |x_1(k)| \le x_1^{\max}, \\ |x_2(k)| \le x_2^{\max}, \\ |f_{pto}(k)| \le f_{pto}^{\max}, \\ \text{The system model in (20) with } \boldsymbol{B_{1dj}}. \end{cases}$$

Therefore, based on the PTO health condition, the proof of **Theorem** 1 has two parts:

A1 HEALTHY PTO ($R(0|k) = 1$)

In this case, $R_j(0|k) = R_{j+1}(0|k) = 1$; therefore, the performance function in (A.1) can be written as:

$$V_1(k) = \boldsymbol{x}^{\mathsf{T}}(N)\boldsymbol{P}\,\boldsymbol{x}(N) + \sum_{k=0}^{N-1} f_{pto}(k)\,\boldsymbol{S}\,\boldsymbol{x}(k) + r\left[f_{pto}(k)\right]^2, \quad \text{(A.2)}$$

where $\boldsymbol{P}$, $\boldsymbol{S}$ and r are constant for all horizons j. In [53], it is proven that $V_1(k)$ is an ISS-Lyapunov function if the following

auxiliary performance function, $V_2(k)$, is an ISS-Lyapunov function:

$$V_2(k) = \boldsymbol{x}^\intercal(N)\boldsymbol{P'}\boldsymbol{x}(N) + \sum_{k=0}^{N-1} f_{pto}(k)\boldsymbol{S}\boldsymbol{x}(k) + r[f_{pto}(k)]^2 + \boldsymbol{x}^\intercal(k+1)\boldsymbol{P''}\boldsymbol{x}(k+1) - \boldsymbol{x}^\intercal(k)\boldsymbol{P''}\boldsymbol{x}(k) + \zeta[f_{ex}(k)]^2, \tag{A.3}$$

where $\zeta > 0$, $\boldsymbol{P'} = \boldsymbol{P} - \boldsymbol{P''} > \boldsymbol{0}$. Also, considering the dissipativity condition in Assumption 1, $\boldsymbol{P''} > \boldsymbol{0}$ is calculated from the following Linear matrix inequality (LMI):

$$\begin{bmatrix} \boldsymbol{A_d}^\intercal \boldsymbol{P''}\boldsymbol{A_d} - \boldsymbol{P''} & \boldsymbol{A_d}^\intercal \boldsymbol{P''}\boldsymbol{B_{1d}} + \boldsymbol{S} \\ \boldsymbol{B_{1d}}^\intercal \boldsymbol{P''}\boldsymbol{A_d} + \boldsymbol{S}^\intercal & \boldsymbol{B_{1d}}^\intercal \boldsymbol{P''}\boldsymbol{B_{1d}} + r \end{bmatrix} > 0. \tag{A.4}$$

For more information, see [28], [53]. Nevertheless, in [53], it is shown that the main condition for $V_2(k)$ to be ISS-Lyapunov is the boundedness of $\boldsymbol{x}^\intercal(k)\boldsymbol{P'}\boldsymbol{x}(k)$ for all horizons j, which is our motivation for the proof procedure in the degrading PTO case.

A2 DEGRADING PTO ($R_j(0|k) = c_j$)

In this case, reliability is fixed inside every horizon, i.e. $R_j(0|k) = c_j > 0$, so $\boldsymbol{P'}_j$ is changing between horizons.

Hence, to focus on the $\boldsymbol{P'}_j$ transition between horizons, if one defines $\boldsymbol{x}_j$ as the state vector for a specific time instant k inside each horizon, the following horizon-varying Lyapunov function can be defined:

$$V_3(j) = \boldsymbol{x}_j^\intercal \boldsymbol{P'}_j \boldsymbol{x}_j, \tag{A.5}$$

Taking the difference of $V_3(j)$ results:

$$\begin{aligned} V_3(j+1) - V_3(j) &= \boldsymbol{x}_{j+1}^\intercal \boldsymbol{P'}_{j+1}\boldsymbol{x}_{j+1} - \boldsymbol{x}_j^\intercal \boldsymbol{P'}_j \boldsymbol{x}_j \\ &= \left(\boldsymbol{x}_{j+1}^\intercal \boldsymbol{P'}_j \boldsymbol{x}_{j+1} - \boldsymbol{x}_j^\intercal \boldsymbol{P'}_j \boldsymbol{x}_j\right) + \boldsymbol{x}_{j+1}^\intercal \left(\boldsymbol{P'}_{j+1} - \boldsymbol{P'}_j\right)\boldsymbol{x}_{j+1}. \end{aligned} \tag{A.6}$$

Since $\boldsymbol{P'}_j$ is fixed in the first term, one can write based on the ISS characteristic discussed in Section A1:

$$\boldsymbol{x}_{j+1}^\intercal \boldsymbol{P'}_j \boldsymbol{x}_{j+1} - \boldsymbol{x}_j^\intercal \boldsymbol{P'}_j \boldsymbol{x}_j \le -\tilde{\alpha}_1 \|\boldsymbol{x}_j\|^2 + \tilde{\alpha}_2 \|f_{exj}\|^2, \tag{A.7}$$

where $\tilde{\alpha}_1, \tilde{\alpha}_2 > 0$. The second term in (A.6) accounts for the variation of $\boldsymbol{P'}_j$ between horizons. Since the reliability metric varies slowly with time and $R_j(0|k) = c_j \in [R_{\min}, 1]$, the map $c_j \mapsto \boldsymbol{P'}_j$ is locally Lipschitz [63] on $[R_{\min}, 1]$. Hence, for some $L_{P'} > 0$ and for all horizons j, if $|c_{j+1} - c_j| \le \rho$ with $\rho > 0$, then

$$\|\boldsymbol{P'}_{j+1} - \boldsymbol{P'}_j\| \le L_{P'}|c_{j+1} - c_j| \le L_{P'}\rho. \tag{A.8}$$

Resulting that

$$\begin{aligned} \boldsymbol{x}_{j+1}^\intercal \left(\boldsymbol{P'}_{j+1} - \boldsymbol{P'}_j\right)\boldsymbol{x}_{j+1} &\le \|\boldsymbol{P'}_{j+1} - \boldsymbol{P'}_j\| \, \|\boldsymbol{x}_{j+1}\|^2 \\ &\le L_{P'}\rho \, \|\boldsymbol{x}_{j+1}\|^2. \end{aligned} \tag{A.9}$$

Moreover, from (20), the closed-loop system can be written as:

$$\boldsymbol{x}_{j+1} = \boldsymbol{A_d}\boldsymbol{x}_j + \boldsymbol{B_{1d}} c_j f_{ptoj}(\boldsymbol{x}_j, f_{exj}) + \boldsymbol{B_{2d}} f_{exj}, \tag{A.10}$$

where the control law is a function of $\boldsymbol{x}_j$ and f_{exj}. Thus, there exist constants $\tilde{\alpha}_3, \tilde{\alpha}_4 > 0$ such that

$$\|\boldsymbol{x}_{j+1}\|^2 \le \tilde{\alpha}_3 \|\boldsymbol{x}_j\|^2 + \tilde{\alpha}_4 \|f_{exj}\|^2. \tag{A.11}$$

Combining this bound with (A.9) yields

$$\boldsymbol{x}_{j+1}^\intercal \left(\boldsymbol{P'}_{j+1} - \boldsymbol{P'}_j\right)\boldsymbol{x}_{j+1} \le L_{P'}\rho\tilde{\alpha}_3 \|\boldsymbol{x}_j\|^2 + L_{P'}\rho\tilde{\alpha}_4 \|f_{exj}\|^2, \tag{A.12}$$

for suitable $\tilde{\alpha}_3, \tilde{\alpha}_4 > 0$. Combining (A.6), (A.7) and (A.12) yields

$$\begin{aligned} V_3(j+1) - V_3(j) &\le (-\tilde{\alpha}_1 + L_{P'}\rho\tilde{\alpha}_3) \, \|\boldsymbol{x}_j\|^2 \\ &+ (\tilde{\alpha}_2 + L_{P'}\rho\tilde{\alpha}_4) \, \|f_{exj}\|^2 = -\alpha\|\boldsymbol{x}_j\|^2 + \gamma\|f_{exj}\|^2, \end{aligned} \tag{A.13}$$

with $\alpha := \tilde{\alpha}_1 - L_{P'}\rho\tilde{\alpha}_3$ and $\gamma := \tilde{\alpha}_2 + L_{P'}\rho\tilde{\alpha}_4$. If, in addition, the controller parameters are chosen such that $L_{P'}\rho\tilde{\alpha}_3 < \tilde{\alpha}_1$, then $\alpha > 0$ and the difference inequality above is the discrete-time ISS-Lyapunov condition. Therefore, $V_3(j)$ is an ISS-Lyapunov function, which completes the proof.

REFERENCES

[1] R. Pelc and R. M. Fujita, "Renewable energy from the ocean," *Mar. Policy*, vol. 26, no. 6, pp. 471–479, 2002.

[2] B. Guo and J. V. Ringwood, "Geometric optimisation of wave energy conversion devices: A survey," *Appl. Energy*, vol. 297, 2021, Art. no. 117100.

[3] B. Reguero, I. Losada, and F. Méndez, "A global wave power resource and its seasonal, interannual and long-term variability," *Appl. Energy*, vol. 148, pp. 366–380, 2015.

[4] H. A. Said, S. Costello, and J. Ringwood, "On the complementarity of wave, tidal, wind and solar resources in Ireland," in *Proc. Eur. Wave Tidal Energy Conf.*, Bilbao, Spain, 2023, vol. 15, pp. 1–6.

[5] H. A. Said, A. Skiarski, and J. V. Ringwood, "Combined renewable resource exploitation: Implications for the all-island Irish electricity supply system," *Energy Convers. Manage.: X*, vol. 26, 2025, Art. no. 100992.

[6] S. Astariz and G. Iglesias, "The economics of wave energy: A review," *Renewable Sustain. Energy Rev.*, vol. 45, pp. 397–408, 2015.

[7] K. Koca et al., "Recent advances in the development of wave energy converters," in *Proc. 9th Eur. Wave Tidal Energy Conf.*, Aalborg, Denmark, 2013, pp. 2–5.

[8] J. V. Ringwood, G. Bacelli, and F. Fusco, "Energy-maximizing control of wave-energy converters: The development of control system technology to optimize their operation," *IEEE Control Syst. Mag.*, vol. 34, no. 5, pp. 30–55, Oct. 2014.

[9] J. V. Ringwood, S. Zhan, and N. Faedo, "Empowering wave energy with control technology: Possibilities and pitfalls," *Annu. Rev. Control*, vol. 55, pp. 18–44, 2023.

[10] B. Teillant, R. Costello, J. Weber, and J. Ringwood, "Productivity and economic assessment of wave energy projects through operational simulations," *Renewable Energy*, vol. 48, pp. 220–230, 2012.

[11] C. Windt, N. Faedo, M. Penalba, F. Dias, and J. V. Ringwood, "Reactive control of wave energy devices–the modelling paradox," *Appl. Ocean Res.*, vol. 109, 2021, Art. no. 102574.

[12] D. Garcıá-Violini, N. Faedo, F. Jaramillo-Lopez, and J. V. Ringwood, "Simple controllers for wave energy devices compared," *J. Mar. Sci. Eng.*, vol. 8, no. 10, 2020, Art. no. 793.

[13] G. Li and M. R. Belmont, "Model predictive control of sea wave energy converters–Part I: A convex approach for the case of a single device," *Renewable Energy*, vol. 69, pp. 453–463, 2014.

[14] Z. Liao, X. Zhang, J. Apsley, M. F. Iacchetti, P. Stansby, and G. Li, "A sea-state-dependent control strategy for wave energy converters: Power limiting in large wave conditions and energy maximising in moderate wave conditions," *IEEE Trans. Sustain. Energy*, vol. 15, no. 3, pp. 1743–1753, Jul. 2024.

[15] J. A. Cretel, G. Lightbody, G. P. Thomas, and A. W. Lewis, "Maximisation of energy capture by a wave-energy point absorber using model predictive control," *IFAC Proc. Volumes*, vol. 44, no. 1, pp. 3714–3721, 2011.

[16] C. Auger, A. Mérigaud, and J. V. Ringwood, "Receding-horizon pseudo-spectral control of wave energy converters using periodic basis functions," *IEEE Trans. Sustain. Energy*, vol. 10, no. 4, pp. 1644–1652, Oct. 2019.

[17] R. Genest and J. V. Ringwood, "Receding horizon pseudospectral control for energy maximization with application to wave energy devices," *IEEE Trans. Control Syst. Technol.*, vol. 25, no. 1, pp. 29–38, Jan. 2017.

[18] N. Faedo, F. J. D. Piuma, G. Giorgi, and J. V. Ringwood, "Nonlinear model reduction for wave energy systems: A moment-matching-based approach," *Nonlinear Dyn.*, vol. 102, no. 3, pp. 1215–1237, 2020.

[19] N. Faedo, G. Scarciotti, A. Astolfi, and J. V. Ringwood, "Nonlinear energy-maximizing optimal control of wave energy systems: A moment-based approach," *IEEE Trans. Control Syst. Technol.*, vol. 29, no. 6, pp. 2533–2547, Nov. 2021.

[20] N. Faedo, G. Giorgi, J. V. Ringwood, and G. Mattiazzo, "Nonlinear moment-based optimal control of wave energy converters with non-ideal power take-off systems," presented at the Int. Conf. Offshore Mechanics Arctic Eng., Hamburg, Germany, Jun. 5–10, 2022, vol. 85932.

[21] M. H. Do and D. Söffker, "State-of-the-art in integrated prognostics and health management control for utility-scale wind turbines," *Renewable Sustain. Energy Rev.*, vol. 145, 2021, Art. no. 111102.

[22] A. Ziaei, H. A. Said, and J. V. Ringwood, "Health-sensitive control of wave energy converters: A primer," *Ocean Eng.*, vol. 311, 2024, Art. no. 118893.

[23] A. Ziaei, H. A. Said, and J. V. Ringwood, "Health aware control of wave energy converters: Possibilities and challenges," in *Proc. 6th Int. Conf. Renewable Energies Offshore*, Lisbon, Portugal, 2024, pp. 1–9.

[24] R. T. Marler and J. S. Arora, "The weighted sum method for multi-objective optimization: New insights," *Struct. Multidisciplinary Optim.*, vol. 41, pp. 853–862, 2010.

[25] A. Ziaei, H. A. Said, and J. V. Ringwood, "Reliability-driven health-aware control augmentation strategies for wave energy converters," *Energy Convers. Manage.: X*, vol. 29, 2025, Art. no. 101501.

[26] A. Ziaei, H. A. Said, and J. V. Ringwood, "Health-aware control augmentation for wave energy converters using a reliability metric," in *Proc. Eur. Wave Tidal Energy Conf.*, Madeira, Portugal, 2025, pp. 1–9.

[27] N. Faedo, S. Olaya, and J. V. Ringwood, "Optimal control, MPC and MPC-like algorithms for wave energy systems: An overview," *IFAC J. Syst. Control*, vol. 1, pp. 37–56, 2017.

[28] S. Zhan, Y. Chen, and J. V. Ringwood, "Terminal weight and constraint design for wave energy converter economic model predictive control problems," *Int. J. Robust Nonlinear Control*, vol. 35, pp. 1–23, 2023.

[29] G. Giorgi and J. V. Ringwood, "Computationally efficient nonlinear Froude–Krylov force calculations for heaving axisymmetric wave energy point absorbers," *J. Ocean Eng. Mar. Energy*, vol. 3, pp. 21–33, 2017.

[30] J. Falnes and A. Kurniawan, *Ocean Waves and Oscillating Systems: Linear Interactions Including Wave-Energy Extraction*, vol. 8. Cambridge, U.K.: Cambridge Univ. Press, 2020.

[31] Z. Yu and J. Falnes, "State-space modelling of a vertical cylinder in heave," *Appl. Ocean Res.*, vol. 17, no. 5, pp. 265–275, 1995.

[32] H. A. Said, D. Garcıá-Violini, and J. V. Ringwood, "Wave-to-grid (W2G) control of a wave energy converter," *Energy Convers. Manage.: X*, vol. 14, 2022, Art. no. 100190.

[33] K. M. Nielsen, T. S. Pedersen, P. Andersen, and S. Ambühl, "Optimizing control of wave energy converter with losses and fatigue in power take off," *IFAC-PapersOnLine*, vol. 50, no. 1, pp. 14680–14685, 2017.

[34] P. Dersin, *Modeling Remaining Useful Life Dynamics in Reliability Engineering*. Boca Raton, FL, USA: CRC Press, 2023.

[35] J. Zhang, T. Liu, and J. Qiao, "Solving a reliability-performance balancing problem for control systems with degrading actuators under model predictive control framework," *J. Franklin Inst.*, vol. 359, no. 9, pp. 4260–4287, 2022.

[36] M. Rausand and A. Hoyland, *System Reliability Theory: Models, Statistical Methods, and Applications*, vol. 396. Hoboken, NJ, USA: Wiley, 2003.

[37] M. Zagorowska, O. Wu, J. R. Ottewill, M. Reble, and N. F. Thornhill, "A survey of models of degradation for control applications," *Annu. Rev. Control*, vol. 50, pp. 150–173, 2020.

[38] Y. Meng, X. Yu, Y. Zhu, and J. Qiao, "Fixed-time attitude control of reusable launch vehicles utilizing reliability-based control allocation," *Control Eng. Pract.*, vol. 151, 2024, Art. no. 106013.

[39] S. Ambühl, M. Kramer, and J. D. Sørensen, "Different reliability assessment approaches for wave energy converters," in *Proc. 11th Eur. Wave Tidal Energy Conf.*, Nantes, France, 2015, pp. 6–11.

[40] J. C. Salazar, A. Sanjuan, F. Nejjari, and R. Sarrate, "Health-aware control of an octorotor UAV system based on actuator reliability," in *Proc. 4th Int. Conf. Control, Decis. Inf. Technol.*, 2017, pp. 815–820.

[41] A. Chamseddine, D. Theilliol, I. Sadeghzadeh, Y. Zhang, and P. Weber, "Optimal reliability design for over-actuated systems based on the MIT rule: Application to an octocopter helicopter testbed," *Rel. Eng. System Saf.*, vol. 132, pp. 196–206, 2014.

[42] X. Yin, X. Zhao, J. Lin, and A. Karcanias, "Reliability aware multi-objective predictive control for wind farm based on machine learning and heuristic optimizations," *Energy*, vol. 202, 2020, Art. no. 117739.

[43] J. C. Salazar, R. Sarrate, F. Nejjari, P. Weber, and D. Theilliol, "Reliability computation within an MPC health-aware framework," *IFAC-PapersOnLine*, vol. 50, no. 1, pp. 12230–12235, 2017.

[44] J. C. Salazar, P. Weber, F. Nejjari, R. Sarrate, and D. Theilliol, "System reliability aware model predictive control framework," *Rel. Eng. System Saf.*, vol. 167, pp. 663–672, 2017.

[45] M. Mueller, R. Lopez, A. McDonald, and G. Jimmy, "Reliability analysis of wave energy converters," in *Proc. 2016 IEEE Int. Conf. Renewable Energy Res. Appl.*, Birmingham, U.K., 2016, pp. 667–672.

[46] S. Zhan, Y. Chen, and J. V. Ringwood, "Terminal weight and constraint design for wave energy converter economic model predictive control problems," *Int. J. Robust Nonlinear Control*, vol. 35, no. 7, pp. 2694–2716, 2025.

[47] G. Bacelli, R. Genest, and J. V. Ringwood, "Nonlinear control of flap-type wave energy converter with a non-ideal power take-off system," *Annu. Rev. Control*, vol. 40, pp. 116–126, 2015.

[48] Z. Lin, J. Zhou, X. Huang, K. Chen, X. Xiao, and J. V. Ringwood, "On loss-aware optimal control of wave energy converters with electrical power take-offs," *IEEE Trans. Sustain. Energy*, vol. 15, no. 4, pp. 2209–2218, Oct. 2024.

[49] S. Butler, F. O'Connor, D. Farren, and J. V. Ringwood, "A feasibility study into prognostics for the main bearing of a wind turbine," in *Proc. IEEE Int. Conf. Control Appl.*, Dubrovnik, Croatia, 2012, pp. 1092–1097.

[50] L.-B. Wu, G.-H. Yang, and D. Ye, "Robust adaptive fault-tolerant control for linear systems with actuator failures and mismatched parameter uncertainties," *IET Control Theory Appl.*, vol. 8, no. 6, pp. 441–449, 2014.

[51] M. Ellis, H. Durand, and P. D. Christofides, "A tutorial review of economic model predictive control methods," *J. Process Control*, vol. 24, no. 8, pp. 1156–1178, 2014.

[52] O. I. Olanrewaju and J. M. Maciejowski, "Implications of dissipativity on stability of economic model predictive control—The indefinite linear quadratic case," *Syst. Control Lett.*, vol. 100, pp. 43–50, 2017.

[53] S. Zhan, W.-H. Chen, T. Steffen, and J. V. Ringwood, "Computationally efficient infinite-horizon indefinite model predictive control with disturbance preview information," *Automatica*, vol. 146, 2022, Art. no. 110667.

[54] G. Papini, B. Paduano, E. Pasta, F. Carapellese, G. Mattiazzo, and N. Faedo, "On the influence of mooring systems in optimal predictive control for wave energy converters," *Renewable Energy*, vol. 218, 2023, Art. no. 119242.

[55] Z.-P. Jiang and Y. Wang, "Input-to-state stability for discrete-time nonlinear systems," *Automatica*, vol. 37, no. 6, pp. 857–869, 2001.

[56] K. Hasselmann et al., "Measurements of wind-wave growth and swell decay during the joint north sea wave project (JONSWAP)," *Ergänzungsheft zur Deutschen Hydrographischen Zeitschrift*, vol. 8, no. 12, pp. 1–95, 1973.

[57] Marine Institute, "AMETS–weather buoy," 2025. Accessed: Nov. 18, 2025. [Online]. Available: https://www.marine.ie/site-area/data-services/real-time-observations/amets-weather-buoy

[58] F. Mosquera, N. Faedo, C. Evangelista, P. Puleston, and J. Ringwood, "Energy-maximising tracking control for a nonlinear heaving point absorber system commanded by second order sliding modes," *IFAC-PapersOnLine*, vol. 55, no. 31, pp. 357–362, 2022.
[59] G. Rinaldi et al., "Multivariate analysis of the reliability, availability, and maintainability characterizations of a spar–buoy wave energy converter farm," *J. Ocean Eng. Mar. Energy*, vol. 4, pp. 199–215, 2018.
[60] M. Kamidelivand et al., "Failure consequence cost analysis of wave energy converters—Component failures, site impacts, and maintenance interval scenarios," *J. Mar. Sci. Eng.*, vol. 12, no. 8, 2024, Art. no. 1251.
[61] A. Mérigaud and J. V. Ringwood, "Free-surface time-series generation for wave energy applications," *IEEE J. Ocean. Eng.*, vol. 43, no. 1, pp. 19–35, Jan. 2018.
[62] M. DeCastro et al., "Evaluating the economic viability of near-future wave energy development along the Galician coast using LCoE analysis for multiple wave energy devices," *J. Cleaner Prod.*, vol. 463, 2024, Art. no. 142740.
[63] Y. Huang, H. Zhang, Y. Shi, J. Z. Kolter, and A. Anandkumar, "Training certifiably robust neural networks with efficient local Lipschitz bounds," in *Proc. Adv. Neural Inf. Process. Syst.*, 2021, vol. 34, pp. 22745–22757.

AMIN ZIAEI (Student Member, IEEE) received the bachelor's degree in electrical engineering from the Sahand University of Technology, Tabriz, Iran, in 2018, and the M.Sc. degree in control engineering from the University of Tabriz, Tabriz, in 2021. His M.Sc. thesis focused on machine-learning-based fault-tolerant control of offshore platforms. He is currently working toward the Ph.D. degree with the Centre for Ocean Energy Research, Maynooth University, Kildare, Ireland. His research interests include control theory, fault-tolerant control, health-aware control, machine learning, wave energy, and health-aware control of wave energy converters.

HAFIZ AHSAN SAID received the B.Sc. degree in electrical engineering from the University of Engineering and Technology Taxila, Taxila, Pakistan, the M.S. degree from the National University of Sciences and Technology, Islamabad, Pakistan, and the Ph.D. degree in electronic engineering from the Centre for Ocean Energy Research (COER), focusing on grid integration aspects of wave energy systems, in 2023. He is currently a Postdoctoral Researcher with COER, working on improving the economic performance of wave energy systems through control methods as part of the Research Ireland SeaChange project. His research interests include wave energy, control applications, and grid integration of renewable energy sources.

JOHN V. RINGWOOD (Life Fellow, IEEE) received the diploma in electrical engineering from Technological University, Dublin, Ireland, in 1981, the M.A. degree in music technology from Maynooth University, Kildare, Ireland, and the Ph.D. degree in control systems from Strathclyde University, Glasgow, U.K., in 1985. From 1985 to 2000, he was with the School of Electronic Engineering, Dublin City University, Dublin. He held visiting positions with Massey University, New Zealand, and The University of Auckland, New Zealand. He was the Founding Head with the Department of Electronic Engineering, Maynooth University. He was also the Dean of engineering from 2001 to 2006. He is currently a Chair Professor of electronic engineering and the Founding Director with the Centre for Ocean Energy Research, Maynooth University. He is also a Chartered Engineer. He is the coauthor of the monograph Hydrodynamic Control of Wave Energy Devices (with Umesh Korde). His research interests include renewable energy systems (and wave energy in particular), physiology, and exercise physiology, and focuses on control systems and its applications. He was the corecipient of the IEEE 2016 Control Systems Outstanding Paper Award and 2023 IEEE Transactions on Control Systems Technology Outstanding Paper Award. He is also an Associate Editor for IEEE TRANSACTIONS ON SUSTAINABLE ENERGY, *Journal of Ocean Engineering and Marine Energy*, and *IET Renewable Power Generation*. He is a Fellow of Engineers Ireland and an IFAC Fellow.